

# Sampling via Stochastic Interpolants by Langevin-based Velocity and Initialization Estimation in Flow ODEs

Chenguang Duan<sup>1</sup>, Yuling Jiao<sup>2</sup>, Gabriele Steidl<sup>3</sup>, Christian Wald<sup>3</sup>, Jerry Zhijian Yang<sup>4</sup>, and Ruizhe Zhang<sup>4</sup>

<sup>1</sup>Institut für Geometrie und Praktische Mathematik, RWTH Aachen University,  
Templergraben 55, 52056 Aachen, Germany.  
duan@igpm.rwth-aachen.de

<sup>2</sup>School of Artificial Intelligence, Wuhan University, Wuhan, Hubei 430072, China.  
yulingjiaomath@whu.edu.cn

<sup>3</sup>Institut für Mathematik, Technische Universität Berlin,  
Straße des 17. Juni 136, 10623 Berlin, Germany.  
{steidl,wald}@math.tu-berlin.de

<sup>4</sup>School of Mathematics and Statistics, Wuhan University, Wuhan, Hubei 430072, China.  
{zjyang.math,ruizhezhang}@whu.edu.cn

January 14, 2026

**Abstract.** We propose a novel method for sampling from unnormalized Boltzmann densities based on a probability-flow ordinary differential equation (ODE) derived from linear stochastic interpolants. The key innovation of our approach is the use of a sequence of Langevin samplers to enable efficient simulation of the flow. Specifically, these Langevin samplers are employed (i) to generate samples from the interpolant distribution at intermediate times and (ii) to construct, starting from these intermediate times, a robust estimator of the velocity field governing the flow ODE. For both applications of the Langevin diffusions, we establish convergence guarantees. Extensive numerical experiments demonstrate the efficiency of the proposed method on challenging multimodal distributions across a range of dimensions, as well as its effectiveness in Bayesian inference tasks.

**Keywords:** sampling, probability flow ODE, Langevin diffusion, stochastic interpolants, log-Sobolev inequality, strong log-concavity

## 1 Introduction

The fundamental goal of sampling involves generating particles from an unnormalized Boltzmann density, serving as a cornerstone in statistical physics (Landau and Binder, 2014; Noè et al., 2019; Midgley et al., 2023; He et al., 2025b), machine learning (Song and Ermon, 2019; Cobb and Jalaian, 2021; Izmailov et al., 2021), and Bayesian inference (Durmus and Moulines, 2019; Overstall et al., 2020; Heng et al., 2021; Stanton et al., 2022; Chung et al., 2023; Ding et al., 2024b; Martin et al., 2025; Chang et al., 2025).

However, sampling becomes difficult when the target distribution is multi-modal. In such scenarios, classical Markov Chain Monte Carlo (MCMC) methods (Gilks et al., 1995), such as Langevin Monte Carlo, Hamiltonian Monte Carlo (HMC) (Hoffman and Gelman, 2014), often fail to explore the global structure of the probability space. They tend to become trapped in local modes, particularly when these modes are separated by high-energy barriers or extensive low-density regions where transitions occur rarely.

A common strategy for sampling from complex multi-modal target distributions is to construct a curve in a measure space that gradually pushes an easy-to-sample initialization distribution to the target distribution. This approach traces its roots to sequential Monte Carlo (SMC) methods (Neal, 2001; Moral et al., 2006), which typically define a sequence of intermediate distributions via a linear interpolation between the target and initialization energy functions. Mathematically, this interpolant scheme corresponds to the normalized product of the target and initialization densities, which is also utilized by Wu et al. (2020); Hagemann et al. (2022); Heng et al. (2021); Wu and Xie (2025); Guo et al. (2025b); Ding et al. (2024b). However, multiplying the target by a Gaussian merely rescales the mode heights without necessarily merging them. Consequently, deep low-density regions separating modes are preserved, potentially causing samplers to become trapped (Chen et al., 2024; He et al., 2025a). Furthermore, because the modes effectively remain distinct until the very end of the annealing process, the necessary mass transport between distant modes is forced to occur at a late stage. This phenomenon is commonly referred to as the “teleportation issue” (Máté and Fleuret, 2023; Chemseddine et al., 2025).

Inspired by diffusion models (Sohl-Dickstein et al., 2015; Ho et al., 2020; Song and Ermon, 2019; Song et al., 2021) and flow-based models (Lipman et al., 2023; Albergo and Vanden-Eijnden, 2023; Albergo et al., 2025), constructing interpolants via Gaussian convolution has garnered significant attention. By convolving the target density with a Gaussian kernel, the energy landscape is effectively smoothed. This process merges isolated modes and populates low-density regions, yielding intermediate distributions that are significantly easier to sample from (Mobahi and Fisher, 2015; Song and Ermon, 2019; Máté and Fleuret, 2023; Chen et al., 2024; He et al., 2025a).

Within the framework of flow-based or diffusion-based sampling methods, the central technical challenge lies in accurately estimating the velocity field that drives the probability flow ODE, or equivalently, the drift term of the associated SDE. In the sampling setting only an unnormalized target density is accessible, making the velocity field or score of the intermediate distributions hard to estimate. Leveraging Tweedie’s formula (Efron, 2011), the velocity field or score function can be expressed as an conditional expectation, enabling on-the-fly Monte Carlo estimation without pre-training a neural network. Existing estimators include importance sampling (Huang et al., 2024a, 2025) and rejection sampling (He et al., 2024). However, these approaches typically suffer in high-dimensional settings due to the curse of dimensionality. An alternative strategy employs Langevin-based methods to estimate the score function (Huang et al., 2024a,b; Grenioux et al., 2024), offering improved scalability in high dimensions.

In this work, we propose a novel framework for sampling from unnormalized Boltzmann densities, driven by linear stochastic interpolants (Albergo and Vanden-Eijnden, 2023; Albergo et al., 2025); see also Wald and Steidl (2025) for an overview. Linear stochastic interpolants induce a probability flow ODE that transports an easy-to-sample initialization distribution to the complex target distribution via Gaussian convolution. Our approach decomposes the intractable problem of sampling from a multi-modal target into a sequence of tractable subproblems, each solvable via Langevin diffusion. Specifically, we employ Langevin diffusion to (i) generate samples from the distribution of an intermediate time of the interpolant, where the distribution is still easy to sample from via Langevin diffusion. Starting from this intermediate time we (ii) use the ODE associated to the interpolant and estimate the vector field using Langevin diffusion as well. In order to improve both (i) and (ii), we apply preconditioning to these Langevin diffusions. This adaptively scales step sizes based on the

local geometry of the distribution, thereby enhancing convergence.

**1.1 Contributions.** Our main contributions are summarized as follows:

- (i) We propose a novel framework for sampling from unnormalized Boltzmann densities based on linear stochastic interpolants. We derive a probability flow ODE framework that transports an initial distribution to the target distribution, where both the generation of initial particles and the estimation of the velocity field are reduced to substantially simpler sampling tasks carried out via Langevin dynamics.
- (ii) We introduce an RMSprop-based preconditioning strategy for Langevin diffusion, which enables adaptive step sizes. This preconditioning improves the ability of the sampler to escape saddle points in complex energy landscapes, thereby enhancing exploration and facilitating transitions across energy barriers. Numerical results demonstrate clear advantages over vanilla Langevin dynamics.
- (iii) We perform extensive numerical experiments to validate the efficiency of the proposed method on multi-modal target distributions in various dimensions. In addition, ablation studies investigate the impact of the initialization time, the necessity of Langevin-based initialization, and the performance gains achieved through preconditioning.

**1.2 Related work.** Unlike our method that estimates velocity fields on-the-fly, a distinct line of research parameterizes these fields using neural networks, leveraging their high expressive power. These approaches, often termed neural samplers (Wu et al., 2020; Arbel et al., 2021; Wang et al., 2026), typically minimize a divergence measure between the parameterized and target distributions.

A natural choice for the training objective is the reverse Kullback-Leibler (KL) divergence, primarily due to its computational tractability. However, training via reverse KL can be unstable when the target distribution is multimodal with high-energy barriers, often resulting in mode collapse. To mitigate this, several alternative objectives have been proposed. For instance, Flow Annealed Importance Sampling Bootstrap (FAB) (Midgley et al., 2023) minimizes the  $\alpha$ -2 divergence. Máté and Fleuret (2023) and Chemseddine et al. (2025) utilize loss functions derived from the residuals of the continuity equation, while Wu and Xie (2025) employ an optimal transport formulation. He et al. (2025a) proposed minimizing the reverse KL divergence along diffusion trajectories to improve mode coverage. In parallel, recent works have focused on constructing neural samplers through the lens of diffusion models and stochastic optimal control (Berner et al., 2024; Zhang and Chen, 2022; Phillips et al., 2024; Liu et al., 2025; Havens et al., 2025; Guo et al., 2025a).

**1.3 Organization.** The remainder of this paper is organized as follows. Section 2 provides a brief introduction to Langevin diffusion and establishes the basic notation used throughout the work. In Section 3, we present the proposed framework for sampling via stochastic interpolants, followed by the Langevin-based velocity field estimation in Section 4. Section 5 details the computational aspects of the flow ODE, including initialization procedures and simulation techniques. To enhance sampling efficiency, we introduce a preconditioning strategy for Langevin diffusion in Section 6. In Section 7, we demonstrate the efficacy of our approach through extensive numerical experiments. Finally, we conclude the paper in Section 8. Detailed proofs and additional experimental settings are provided in the appendices.

## 2 Preliminaries

Our approach is heavily based on the Langevin diffusion

$$(2.1) \quad dU_s = \nabla \log p(U_s) ds + \sqrt{2} dB_s, \quad s \geq 0.$$

starting in the random variable  $U_0 \in \mathbb{R}^d$  with score function  $\nabla \log p$ . Here  $B_s$  denotes the  $d$ -dimensional Brownian motion. Under some assumptions on the density  $p$ , we have that the marginals  $U_s$  converge for  $s \rightarrow \infty$  in distribution to a random variable with law  $p$ . To this end, recall that a density  $p$  satisfies a *log-Sobolev inequality* with constant  $C_{\text{LSI}}(p)$ , if for all  $f \in C_b^\infty(\mathbb{R}^d)$ ,

$$\text{Ent}_p(f^2) \leq 2C_{\text{LSI}}(p) \mathbb{E}_p |\nabla f|^2 \quad \text{for all } f \in C_b^\infty(\mathbb{R}^d),$$

where  $\text{Ent}$  is the entropy defined as

$$\text{Ent}_p(f^2) := \int f^2 \log \frac{f^2}{\mathbb{E}_p[f^2]} p dx.$$

A density  $p \in C^2(\mathbb{R})$  is called  $\beta$ -strongly log-concave with some  $\beta > 0$ , if the Hessian of its logarithm fulfills  $\beta I_d \preceq -\nabla^2 \log p$ . By the result of Bakry–Émery (Bakry and Émery, 1985) a  $\beta$ -strongly log-concave density satisfies a log-Sobolev inequality with a constant  $\beta^{-1}$ .

The *Kullback-Leibler (KL) divergence* of two densities  $p$  and  $q$  is defined by  $\text{KL}(p, q) := \int \log \left( \frac{p}{q} \right) p dx$ , if  $q(x) = 0$  implies  $p(x) = 0$  a.e., and otherwise by  $\text{KL}(p, q) := +\infty$ .

Then the following theorem was proved in Vempala and Wibisono (2019) and Bakry and Émery (1985), see also the recent paper Chewi et al. (2025).

**Theorem 2.1.** *Let  $U_s$  with law  $p_{U_s}$  be generated by (2.1) with an arbitrary initial distribution  $p_{U_0}$ . Then the following holds true.*

i) *If  $p$  satisfies a log-Sobolev inequality with constant  $C_{\text{LSI}}(p)$ , then*

$$\text{KL}(p_{U_s}, p) \leq e^{-\frac{2s}{C_{\text{LSI}}(p)}} \text{KL}(p_{U_0}, p),$$

ii) *If  $p$  is  $\beta$ -strongly log-concave, then*

$$\text{KL}(p_{U_s}, p) \leq e^{-2s\beta} \text{KL}(p_{U_0}, p).$$

In the following, we denote by  $\gamma_{\sigma^2}$  the density of the normal distribution  $\mathcal{N}(0, \sigma^2 I_d)$  with mean zero and variance  $\sigma^2 > 0$ , and set  $\gamma := \gamma_1$  for the density of the standard normal distribution. Further,  $\Xi$  always denotes a standard normal distributed random variable, so that  $\sigma \Xi$ ,  $\sigma \neq 0$  has density  $\gamma_{\sigma^2}$ . Recall that for two independent random variables  $X$  and  $Z$  with densities  $p_X$  and  $p_Z$ , resp., the random variable  $aX + bZ$ ,  $a, b \in \mathbb{R} \setminus \{0\}$  has the density

$$(2.2) \quad p_{aX+bZ} = p_{aX} * p_{bZ} = \int p_X(a^{-1}x) p_Z(b^{-1}(\cdot - x)) dx.$$

In particular, the convolution of two Gaussians  $\mathcal{N}(m, \sigma^2)$  and  $\mathcal{N}(\tilde{m}, \tilde{\sigma}^2)$  results in the Gaussian  $\mathcal{N}(m + \tilde{m}, \sigma^2 + \tilde{\sigma}^2)$ .

### 3 Sampling via Stochastic Interpolants

To sample from a potentially complex target distribution  $p_{X_1}$ , we consider the stochastic process (linear interpolant (Albergo and Vanden-Eijnden, 2023; Albergo et al., 2025)) for  $(X_0, X_1) \sim \gamma \otimes p_{X_1}$  defined by

$$(3.1) \quad X_t = tX_1 + (1-t)X_0, \quad t \in (0, 1).$$

This evolution is governed by a **continuity equation**

$$(3.2) \quad \partial_t p_{X_t}(x) + \nabla \cdot (u(t, x)p_{X_t}(x)) = 0, \quad t \in (0, 1),$$

where the velocity field  $u : \mathbb{R} \times \mathbb{R}^d \rightarrow \mathbb{R}^d$  is defined as

$$(3.3) \quad u(t, x) := \mathbb{E}[X_1 - X_0 | X_t = x] = -\frac{1}{1-t}x + \frac{1}{1-t}\mathbb{E}[X_1 | X_t = x],$$

see Ambrosio et al. (2005); Liu et al. (2023). Note that  $\|u\|_{L^2(p_t)} \in L^1([0, 1])$  is always true for a curve of type (3.1), see Wald and Steidl (2025, Theorem 4.6 and Corollary 6.4). Conditioned on  $X_1 = x_1$ , the density of the interpolant  $X_t$  is given as

$$p_{X_t|X_1=x_1} = \gamma_{(1-t)^2}(\cdot - tx_1),$$

and by the law of total probability we have

$$(3.4) \quad p_{X_t} := \int p_{X_t|X_1=x_1} p_{X_1}(x_1) dx_1 = \int \gamma_{(1-t)^2}(\cdot - tx_1) p_{X_1}(x_1) dx_1.$$

Moreover, we have the important relation between the score of  $p_{X_t}$  and the velocity field

$$(3.5) \quad \nabla \log p_{X_t}(x_t) = \frac{t}{1-t}u(t, x_t) - \frac{1}{1-t}x_t, \quad t \in (0, 1),$$

see, e.g. Zhang et al. (2024, Appendix A1), Wald and Steidl (2025, Remark 6.5) and Ding et al. (2024a, Proposition 3.1).

Let  $T_0 \in (0, 1)$  be a fixed starting time point. The characteristic curves of the continuity equation (3.2) define a flow map  $\psi : (T_0, 1) \times \mathbb{R}^d \rightarrow \mathbb{R}^d$ , specified by the following **probability flow ODE**:

$$(3.6) \quad \begin{aligned} \frac{d}{dt} \psi(t, x) &= u(t, \psi(t, x)), \quad t \in (T_0, 1), \\ \psi(T_0, x) &= x. \end{aligned}$$

If

$$(3.7) \quad \int_0^1 \sup_B \{\|u(t, \cdot)\| + \text{Lip}(u(t, \cdot), B)\} dt < \infty \text{ for all compact } B \subset \mathbb{R}^d,$$

then the ODE has a unique solution, see Ambrosio et al. (2005, Proposition 8.1.8). Further, it holds that if  $X_{T_0} \sim p_{X_{T_0}}$ , then  $\psi(t, X_{T_0}) \sim p_{X_t}$ , which implies

$$p_{X_t} = \psi(t, \cdot) \# p_{X_{T_0}} := p_{X_{T_0}} \circ \psi(t, \cdot)^{-1}, \quad t \in (T_0, 1).$$

Our sampling algorithm via the flow ODE is based on the observation that intuitively, the Gaussian-convolved distribution  $p_{X_{T_0}}$  in (3.4) is already much easier to sample than the original distribution  $p_{X_1}$ , when  $T_0$  is small. Let us illustrate this by the following example.

*Example 3.1* (Gaussian mixture). Consider a mixture of two 1-dimensional Gaussians

$$p_{X_1}(x_1) = \frac{1}{2}\gamma(x_1 - m) + \frac{1}{2}\gamma(x_1 + m)$$

with a constant  $m > \sqrt{2}$ . Then, the marginal density of the interpolant is the Gaussian mixture

$$\begin{aligned} p_{X_t}(x_t) &= \frac{1}{2} \int \gamma_{(1-t)^2}(x_t - tx_1) \gamma(x_1 - m) dx_1 + \frac{1}{2} \int \gamma_{(1-t)^2}(x_t - tx_1) \gamma(x_1 + m) dx_1 \\ (3.8) \quad &= \frac{1}{2} \gamma_{\sigma_t^2}(x_t - mt) + \frac{1}{2} \gamma_{\sigma_t^2}(x_t + mt), \quad \sigma_t^2 := t^2 + (1-t)^2. \end{aligned}$$

Differentiating with respect to  $x$  yields

$$\frac{dp_{X_t}(x)}{dx} = -\frac{1}{2\sigma_t^2 \sqrt{2\pi\sigma_t^2}} \left( (x - mt)e^{-\frac{(x-mt)^2}{2\sigma_t^2}} + (x + mt)e^{-\frac{(x+mt)^2}{2\sigma_t^2}} \right),$$

so that critical points have to fulfill  $(x - mt)e^{-\frac{(x-mt)^2}{2\sigma_t^2}} = -(x + mt)e^{-\frac{(x+mt)^2}{2\sigma_t^2}}$ , which simplifies to the transcendental equation  $x = mt \tanh\left(\frac{mtx}{\sigma_t^2}\right)$ . While  $x = 0$  is always a solution, non-zero solutions indicating bimodality emerge when the curvature at the origin becomes positive, i.e., when the squared mean exceeds the variance  $\sigma_t^2$ . Thus, we obtain

$$(mt)^2 > \sigma_t^2 \iff (m^2 - 2)t^2 + 2t - 1 > 0.$$

Solving for root in  $(0, 1)$ , we find the distribution transitions from unimodal to bimodal at

$$t^* = \frac{\sqrt{m^2 - 1} - 1}{m^2 - 2}.$$

Crucially, the interpolant density  $p_{X_t}$  remains unimodal for all  $t \in (0, t^*]$  which is a key property, see Figure 1.  $\square$

Based on the above observation, depending on some critical hyperparameter  $T_0 \in (0, 1)$ , we propose the following **sampling strategy**.

**1. Velocity Field Estimator:** For any  $t \in [T_0, 1)$  and any  $x_t \in \mathbb{R}^d$ , we propose the construction of an estimator  $\hat{u}(t, x_t)$  of the velocity field  $u(t, x_t)$  based on (3.3) by approximating  $\mathbb{E}[X_1 | X_t = x_t]$  using samples from  $p_{X_1 | X_t = x_t}$ . These samples are provided by the Euler-Maruyama scheme of the Langevin diffusion

$$dZ_s = \nabla \log p_{X_1 | X_t = x_t}(Z_s) ds + \sqrt{2} dB_s, \quad s \geq 0,$$

**2. Computation of Flow ODE:** Having such an estimator at hand, it is used twofold, namely to sample from the initial distribution  $p_{X_{T_0}}$  of our flow ODE (3.6) and to compute the sample flow itself.

i) **Flow Initialization:** We apply the Langevin diffusion

$$dU_s = \nabla \log p_{X_{T_0}}(U_s) dr + \sqrt{2} dB_s, \quad s \geq 0.$$

starting in a standard normal distribution  $U_0 \sim \mathcal{N}(0, \mathbf{I}_d)$ . Using our estimator  $\hat{u}(T_0, \cdot)$ , the score  $\nabla \log p_{X_{T_0}}$  can be simply estimated via (3.5).

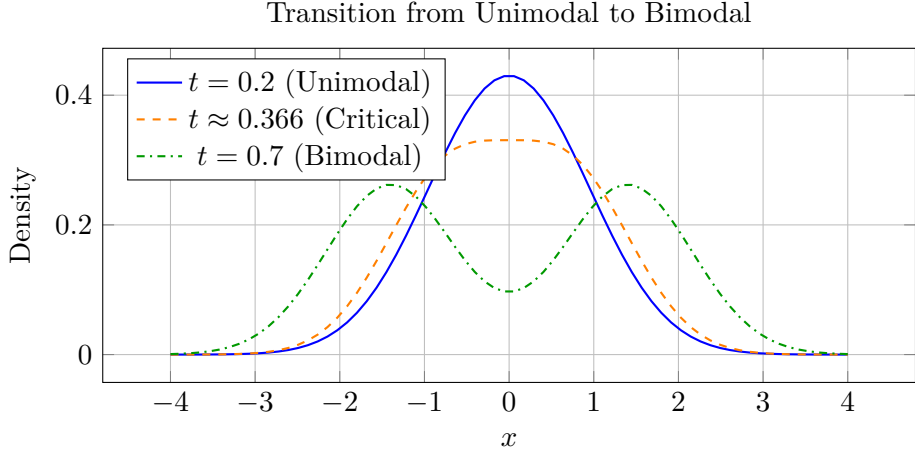


Figure 1: Density  $p_{X_t}$  in (3.8) with  $m = 2$  at three time points, illustrating the pitchfork bifurcation.

ii) **Sampling via Flow ODE:** Having an estimator for the flow field  $\hat{u}$  we can successive run the time discrete flows ODE (3.6) starting in samples of  $p_{X_{T_0}}$ .

In the following sections, we describe our strategy in detail including convergence results.

We adopt a Gaussian convolution assumption standard, see e.g. [Saremi et al. \(2024\)](#); [Grenioux et al. \(2024\)](#); [Ding et al. \(2024a\)](#); [Beyler and Bach \(2025\)](#).

**Assumption 1.** There exists a random variable  $Y \in \mathbb{R}^d$  with law  $p_Y$ , where

$$\text{supp}(p_Y) \subseteq B(0, R) := \{y \in \mathbb{R}^d : \|y\|_2 \leq R\}, \quad R > 0,$$

so that  $X_1 = Y + \sigma \Xi$ ,  $\sigma^2 > 0$ , i.e., the target density fulfills

$$p_{X_1} = \int \gamma_{\sigma^2}(\cdot - y) p_Y(y) dy.$$

The following result from [Chen et al. \(2021, Corollary 1\)](#) states that  $X_1$  satisfies a log-Sobolev inequality.

**Lemma 3.2.** *Let  $p$  be a density with  $\text{supp}(p) \subseteq B(0, R)$ . Then, for any  $\sigma^2 \in (0, 1)$ , the density  $p * \gamma_{\sigma^2}$  fulfills a log-Sobolev inequality with constant*

$$C_{\text{LSI}}(p * \gamma_{\sigma^2}) \leq 6(4R^2 + \sigma^2) e^{\frac{4R^2}{\sigma^2}} = 6\sigma^2 \left(1 + \frac{4R^2}{\sigma^2}\right) e^{\frac{4R^2}{\sigma^2}} \leq 6 e^{\frac{8R^2}{\sigma^2}}.$$

## 4 Velocity Field Estimator

According to (3.3), estimating the velocity field  $u(t, \cdot)$  of the flow ODE reduces to estimating the conditional expectation of  $X_1$  given  $X_t = x_t$ . By Bayes' rule, we know that

$$\begin{aligned} p_{X_1|X_t=x_t} &= \frac{1}{p_{X_t}} \gamma_{(1-t)^2}(x_t - t \cdot) p_{X_1} \\ (4.1) \quad &= \frac{1}{p_{X_t}} \exp \left\{ -\frac{\|x_t - t \cdot\|_2^2}{2(1-t)^2} + \log p_{X_1} \right\}. \end{aligned}$$

For a fixed  $x_t \in \mathbb{R}^d$ , the Langevin diffusion admitting  $p_{X_1|X_t=x_t}$  as its invariant distribution is given by

$$(4.2) \quad dZ_s^{t,x_t} = \nabla \log p_{X_1|X_t=x_t}(Z_s^{t,x_t}) ds + \sqrt{2} dB_s, \quad s \geq 0.$$

For simplicity of notation, we write  $Z_s$  instead of  $Z_s^{t,x_t}$  if the conditioning on  $X_t = x_t$  is clear from the context. By (4.1), the score function reads as

$$(4.3) \quad \nabla \log p_{X_1|X_t=x_t}(x_1) = \frac{t(x_t - tx_1)}{(1-t)^2} + \nabla \log p_{X_1}(x_1).$$

Langevin diffusions involving this type of score have previously been investigated in the context of proximal sampling, parallel tempering and annealed Langevin diffusion, e.g., in [Lee et al. \(2021\)](#); [Dong and Tong \(2022\)](#); [Guo et al. \(2025b\)](#).

Under mild assumptions, the Langevin diffusion (4.2) converges to the denoising distribution (4.1).

**Proposition 4.1.** *Let Assumption 1 be fulfilled, and let  $X_t$  be given by the linear interpolant (3.1). For  $t \in (0, 1)$  and  $\sigma^2 > 0$ , set*

$$\beta_t := \frac{t^2}{(1-t)^2} + \frac{1}{\sigma^2} - \frac{R^2}{\sigma^4}.$$

*Then, for every  $t \in (0, 1)$ , it holds*

$$\beta_t \mathbf{I}_d \preceq -\nabla^2 \log p_{X_1|X_t=x_t} \preceq \left( \beta_t + \frac{R^2}{\sigma^4} \right) \mathbf{I}_d,$$

*and  $p_{X_1|X_t=x_t}$  is  $\beta_t$ -strongly log-concave for  $t \in (T^*, 1)$ , where*

$$(4.4) \quad T^* = \begin{cases} 0 & \text{if } R^2 \leq \sigma^2 \\ \frac{1}{2} & \text{if } R^2 = \sigma^2 + \sigma^4, \\ \frac{R^2 - \sigma^2 - \sigma^2 \sqrt{R^2 - \sigma^2}}{R^2 - \sigma^2 - \sigma^4} & \text{otherwise.} \end{cases}$$

*We have  $T^* < \frac{1}{2}$  if  $\sigma^2 < R^2 < \sigma^2 + \sigma^4$ , and  $T^* > \frac{1}{2}$  if  $R^2 > \sigma^2 + \sigma^4$ .*

*Further, for  $t \in (T^*, 1)$ , it holds*

$$(4.5) \quad \text{KL} \left( p_{Z_s}, p_{X_1|X_t=x_t} \right) \leq e^{-2\beta_t s} \text{KL} \left( p_{Z_0}, p_{X_1|X_t=x_t} \right).$$

*where  $Z_s$ ,  $s \geq 0$  is defined by the Langevin diffusion (4.2).*

The proof is given in Appendix B.

The proposition indicates that the denoising density  $p_{X_1|X_t=x_t}$  becomes  $\beta_t$ -strongly log-concave with a larger  $\beta_t$  as  $t$  increases. Specifically, in the over-smoothed regime, i.e.,  $R^2 \leq \sigma^2$ , the denoising density is log-concave for all  $t \in (0, 1)$ . In contrast, in the under-smoothed regime,  $R^2 > \sigma^2$ , to ensure the log-concavity of the denoising density for any  $t \in (T^*, 1)$ , we cannot allow the initial time  $T_0$  in the next section to approach zero.

**Euler-Maruyama scheme.** Although the convergence of the Langevin diffusion (4.2) is theoretically guaranteed, analytical simulation is intractable, necessitating Euler-Maruyama time-discretization. Let  $\eta > 0$  denote the step size, and consider the time partition  $0 < \eta < \dots < K\eta$ . Solving the SDE (4.2) with the Euler-Maruyama scheme results in

$$(4.6) \quad \bar{Z}_{(k+1)\eta} = \bar{Z}_{k\eta} + \eta \nabla \log p_{X_1|X_t=x_t}(\bar{Z}_{k\eta}) + \sqrt{2\eta} \xi_k, \quad \xi_k \sim \mathcal{N}(0, I_d).$$

This scheme is also known as Langevin Monte Carlo (LMC) or unadjusted Langevin algorithm (ULA). Using Proposition 4.1 we can conclude that, if we start with particles  $\bar{Z}_0^1, \dots, \bar{Z}_0^n$  drawn from some distribution  $p_{Z_0}$  in (4.6), we obtain

$$\frac{1}{n} \sum_{i=1}^n \bar{Z}_{K\eta}^i \approx \mathbb{E}[X_1|X_t=x_t].$$

**Monte Carlo approximation of the velocity.** Using (3.3) and samples  $\{\bar{Z}_{K\eta}^i\}_{i=1}^n$ , we propose the following estimator of the velocity field:

$$(4.7) \quad \hat{u}(t, x_t) := -\frac{1}{1-t} x_t + \frac{1}{1-t} \frac{1}{n} \sum_{i=1}^n \bar{Z}_{K\eta}^i \approx u(t, x_t).$$

*Remark 4.2* (Early-stopping). Note that both the denoising score  $\nabla \log p_{X_1|X_t=x_t}$  in (4.3) and the velocity estimator  $\hat{u}(t, \cdot)$  in (4.7) explode for  $t$  close to 1. Hence, we employ an early-stopping in the simulation of probability flow ODE (3.6). Specifically, we need to terminate the simulating at a terminal time  $T_{\text{end}} < 1$  to ensure numerical stability. In Appendix C, we show how this can be avoided by a **rescaling method**.

The complete algorithm is summarized in Algorithm 1.

---

**Algorithm 1:** Velocity field estimator by Monte Carlo-Langevin
 

---

**Input:** Time and location of interest  $(t, x_t)$ , target score  $\nabla \log p_{X_1}$ , step size  $\eta$ , and number of steps  $K$ .

**Output:** Estimator  $\hat{u}(t, x_t) \approx u(t, x_t)$ .

```

1 Initialize particles:  $\bar{Z}_0^1, \dots, \bar{Z}_0^n$ .
2 for  $k \in \{0, \dots, K-1\}$  do
3   # Calculate the denoising score
4    $s_{k+1}^i \leftarrow -\frac{t^2}{(1-t)^2} \bar{Z}_{k\eta}^i + \frac{t}{(1-t)^2} x_t + \nabla \log p_{X_1}(\bar{Z}_{k\eta}^i)$  for  $1 \leq i \leq n$ .
5   # Langevin update
6    $\bar{Z}_{(k+1)\eta}^i \sim \mathcal{N}(\bar{Z}_{k\eta}^i + \eta s_{k+1}^i, 2\eta I_d)$  for  $1 \leq i \leq n$ .
7 end
8 # Monte Carlo estimation
9  $\hat{u}(t, x_t) = -\frac{1}{1-t} x_t + \frac{1}{1-t} \frac{1}{n} \sum_{i=1}^n \bar{Z}_{K\eta}^i$ .
10 return  $\hat{u}(t, x_t)$ 

```

---

**Initialization of Langevin sampling.** By Proposition 4.1 the convergence of the Langevin diffusion (4.2) depends on the quality of the initialization distribution  $p_{Z_0}$ . This necessitates selecting an initial distribution that approximates the target density  $p_{X_1|X_t=x_t}$  as closely as possible.

We employ importance sampling (Neal, 2001). Specifically, we utilize the Gaussian  $\mathcal{N}(t^{-1}x_t, (1-t)^2t^{-2}\mathbf{I}_d)$  as the proposal distribution, and treat the density  $p_{X_1}$  of the target distribution as the weight function:

$$(4.8) \quad p_{X_1|X_t=x_t} \propto \underbrace{p_{X_1}(x_1)}_{\text{weight}} \underbrace{\gamma_{(1-t)^2t^{-2}}(x_1 - t^{-1}x_t)}_{\text{proposal}}.$$

We first take i.i.d. samples  $Z^1, \dots, Z^n$  from the Gaussian proposal distribution. By substituting the proposal distribution with its sample approximation and applying (4.8), we obtain the empirical approximation of the denoising distribution

$$\hat{p}_{X_1|X_t=x_t} := \sum_{i=1}^n \frac{p_{X_1}(Z^i)}{\sum_{k=1}^n p_{X_1}(Z^k)} \delta_{Z^i}.$$

This empirical measure  $\hat{p}_{X_1|X_t=x_t}$  converges to the denoising distribution  $p_{X_1|X_t=x_t}$  as the number of samples  $n$  approaches infinity (Neal, 2001). By resampling from this empirical measure, we generate particles that approximately follow the denoising distribution, providing a suitable initialization for Langevin sampling.

## 5 Computation of Flow ODE

Based on the velocity field estimator constructed in the previous section, we can handle the flow ODE. We start with the initialization, i.e. sampling from  $p_{X_{T_0}}$ , where  $T_0 > T^*$  and consider the flow ODE numerically afterwards.

**5.1 Flow Initialization.** Langevin diffusion admitting  $p_{X_{T_0}}$  as its invariant distribution reads as

$$(5.1) \quad dU_s = \nabla \log p_{X_{T_0}}(U_s) ds + \sqrt{2} dB_s, \quad s \geq 0.$$

In practice, we initialize  $U_0$  by the standard Gaussian distribution  $\mathcal{N}(0, \mathbf{I}_d)$ . For  $T_0 > T^*$ , we apply a score estimator based on the velocity estimator (4.7) and (3.5) by

$$(5.2) \quad \hat{s}(T_0, x_{T_0}) = \frac{T_0}{1-T_0} \hat{u}(T_0, x_{T_0}) - \frac{1}{1-T_0} x_{T_0}.$$

Let  $\tau > 0$  be the step size, and let  $L$  be the number of steps. The, applying the Euler-Maruyama discretization with step size  $\tau > 0$  and  $L$  steps yields

$$(5.3) \quad \hat{U}_{(\ell+1)\tau} = \hat{U}_{\ell\tau} + \tau \hat{s}(T_0, \hat{U}_{\ell\tau}) + \sqrt{2\tau} \zeta_\ell, \quad \zeta_\ell \sim \mathcal{N}(0, I_d), \quad 0 \leq \ell \leq L-1.$$

The resulting particle  $\hat{U}_{L\tau}$  approximates  $p_{X_{T_0}}$ , thereby serving as the initialization for the probability flow ODE (3.6). The initialization algorithm of initialization is summarized in Algorithm 2.

By following proposition,  $p_{U_s}$  converges exponentially to the invariant distribution  $p_{X_{T_0}}$ .

**Proposition 5.1.** *Let Assumption 1 be fulfilled. Let  $p_{X_{T_0}}$  be the distribution defined by (3.4) and let  $U_s$  be given by in (5.1). Then, for every  $s > 0$ , it holds*

$$\text{KL}\left(p_{U_s}, p_{X_{T_0}}\right) \leq \exp\left\{-\frac{s}{3} \exp\left\{-\frac{8T_0^2 R^2}{(1-T_0(1-\sigma))^2}\right\}\right\} \text{KL}\left(p_{U_0}, p_{X_{T_0}}\right).$$

---

**Algorithm 2:** Initialization of probability flow ODE

---

**Input:** The initialization time  $T_0$ , the step size  $\tau$ , and the number of steps  $L$ .

**Output:** Particle  $\hat{U}_{L\tau}$  approximately following  $p_{X_{T_0}}$ .

---

```

1 Initialize particle:  $\hat{U}_0 \sim \mathcal{N}(0, \mathbf{I}_d)$ .
2 for  $\ell \in \{0, \dots, L-1\}$  do
3   # Score estimation
4   Calculate the velocity estimator  $\hat{u}(T_0, \hat{U}_{\ell\tau})$  using Algorithm 1.
5   Calculate the score estimator  $\hat{s}(T_0, \hat{U}_{\ell\tau})$  using (5.2).
6   # Langevin update
7    $\hat{U}_{(\ell+1)\tau} \sim \mathcal{N}(\hat{U}_{\ell\tau} + \tau \hat{s}(T_0, \hat{U}_{\ell\tau}), 2\tau \mathbf{I}_d)$ .
8 end
9 return  $\hat{U}_{L\tau}$ 

```

---

*Proof.* By assumptions we have

$$X_{T_0} = T_0 X_1 + (1 - T_0) X_0 \stackrel{d}{=} T_0(Y + \sigma \Xi) + (1 - T_0) X_0 \stackrel{d}{=} T_0 Y + (1 - T_0(1 - \sigma)) \Xi.$$

This is a convolution of a density with support in the ball of radius  $T_0 R$  and a Gaussian of variance  $(1 - T_0(1 - \sigma))^2 \in (0, 1)$ . Thus, by Lemma 3.2, we conclude

$$(5.4) \quad C_{\text{LSI}}(p_{X_{T_0}}) \leq 6 \exp \left\{ \frac{8T_0^2 R^2}{(1 - T_0(1 - \sigma))^2} \right\}$$

and the assertion follows by Theorem 2.1 i).  $\square$

The proposition suggests that the Langevin diffusion (5.1) converges more rapidly when  $T_0/(1 - T_0(1 - \sigma))$  is small, i.e.,  $T_0$  is small. Combining Propositions 4.1 and 5.1 reveals a trade-off in the selection of  $T_0$ : while a larger initial time  $T_0$  accelerates the convergence of (4.2), it hinders the convergence of (5.1).

The following remark underlines the intuition from Example 3.1 that  $p_{T_0}$  is significantly better tractable by Langevin diffusion than the target distribution  $p_{X_1}$ .

*Remark 5.2* (Regularizing effect of Gaussian convolution). By Assumption 1 and Lemma 3.2 the target distribution  $p_{X_1}$  satisfies a log-Sobolev inequality with constant  $C_{\text{LSI}}(p_{X_1}) \leq 6 e^{\frac{8R^2}{\sigma^2}}$ ,  $\sigma \in (0, 1)$ . By Theorem 2.1 i), this provides an exponential convergence of the Langevin dynamics

$$dU_s = \nabla \log p_{X_1}(U_s) \, ds + \sqrt{2} \, dB_s, \quad s \geq 0$$

towards the invariant distribution  $p_{X_1}$ . However, for a fixed initialization time  $T_0 \in (0, 1)$ , the  $C_{\text{LSI}}(p_{X_{T_0}})$  in (5.4) is significantly smaller than  $C_{\text{LSI}}(p_{X_1})$ , since

$$\frac{1}{\sigma} > \frac{T_0}{1 - T_0(1 - \sigma)}$$

and the right-hand side becomes smaller the smaller  $T_0 \in (T^*, 1)$  is. In particular, in the regime where  $\sigma$  is small the Langevin dynamics towards  $p_{X_{T_0}}$  converges much faster making sampling more efficient.

**5.2 Sampling via Flow ODE.** Once we can sample from our initial distribution  $p_{T_0}$  and have an estimator for the velocity field, we can employ an Euler discretization of the ODE (3.6) to obtain a practical sampling scheme. According to (4.7), we terminate the simulation of probability flow ODE at an early-stopping time  $T_{\text{end}} < 1$  to ensure numerical stability. For a total number  $M$  of discretization steps, we choose the step size  $h := (T_{\text{end}} - T_0)/M$ , and set  $t_m := T_0 + mh$ ,  $0 \leq m \leq M$ . Then the discrete-time flow  $\hat{\psi}$  advances the particles in each time step by

$$(5.5) \quad \begin{aligned} \hat{\psi}(t_{m+1}, x_{T_0}) &= \hat{\psi}(t_m, x_{T_0}) + h\hat{u}(t_m, \hat{\psi}(t_m, x_{T_0})), \\ \hat{\psi}(T_0, x_{T_0}) &= x_{T_0}. \end{aligned}$$

Under mild assumptions, the induced pushforward distribution  $(\hat{\psi}(T_{\text{end}}, \cdot))_{\sharp}p_{T_0}$  approximates the target distribution  $p_{X_1} \approx p_{X_{T_{\text{end}}}}$ , provided the velocity estimation errors is sufficiently small. Incorporating the initialization mechanism from Section 5.1, the complete sampling pipeline is given by

$$\hat{X}_{T_{\text{end}}} := \hat{\psi}(T_{\text{end}}, \hat{X}_{T_0}), \quad \hat{X}_{T_0} := \hat{U}_{L\tau},$$

where the samples  $\hat{X}_{T_0}$  serve as the starting point for the ODE integration, and  $\hat{U}_{L\tau}$  is defined in (5.3). The full sampling procedure is summarized in Algorithm 3.

---

**Algorithm 3:** Sampling via probability flow ODE

---

**Input:** The initial time  $T_0$ , the terminal time  $T_{\text{end}}$ , and the number of steps  $M$ .  
**Output:** Particle  $\hat{\psi}(T_{\text{end}}, \hat{X}_{T_0})$  approximately following  $p_{X_{T_{\text{end}}}} \approx p_{X_1}$ .

- 1 Calculate the step size:  $h = (T_{\text{end}} - T_0)/M$ .
- 2 Generate time points:  $t_m = T_0 + mh$  for  $0 \leq m \leq M$ .
- 3 Initialize particle  $\hat{\psi}(t_0, \hat{X}_{T_0}) = \hat{X}_{T_0} \leftarrow \hat{U}_{L\tau}$  using Algorithm 2.
- 4 **for**  $m \in \{0, \dots, M - 1\}$  **do**
- 5   **# Velocity estimation**
- 6   Calculate the velocity estimator  $\hat{u}(t_m, \hat{\psi}(t_m, \hat{X}_{T_0}))$  using Algorithm 1.
- 7   **# Flow update**
- 8    $\hat{\psi}(t_{m+1}, \hat{X}_{T_0}) \leftarrow \hat{\psi}(t_m, \hat{X}_{T_0}) + h\hat{u}(t_m, \hat{\psi}(t_m, \hat{X}_{T_0})).$
- 9 **end**
- 10 **return**  $\hat{\psi}(T_{\text{end}}, \hat{X}_{T_0})$

---

**Well-Posedness of the Flow ODE.** Finally, we verify that the condition (3.7) is fulfilled. Clearly, it suffices to prove that  $\nabla u(t, x)$  is bounded for all  $t \in (0, 1)$  and all  $x \in \mathbb{R}^d$ . Indeed, following similar lines as in the paper Ding et al. (2024a) of some of the authors, we have the following results which proofs can be found for convenience in the appendix.

**Lemma 5.3** (Linear growth of velocity field). *Let Assumption 1 be fulfilled. For every  $t \in (0, 1)$ , it holds*

$$\|u(t, x_t)\|_2 \leq B(1 + \|x_t\|_2), \quad x_t \in \mathbb{R}^d,$$

where  $B$  is a constant only depending on  $\sigma$  and  $R$ .

**Theorem 5.4** (Lipschitz continuity of velocity field). *Let Assumption 1 be fulfilled. For every  $t \in (0, 1)$ , it holds*

$$\|\nabla u(t, x_t)\|_{\text{op}} \leq G, \quad x_t \in \mathbb{R}^d,$$

where  $G$  is a constant only depending on  $\sigma$  and  $R$ .

## 6 Preconditioned Langevin Algorithm

Although we have established convergence of the Langevin diffusion for velocity estimation (4.2) and for initialization (5.1), the convergence behavior can be further improved through preconditioning, for the following reasons:

- (i) For a log-concave target distribution, the convergence rate of Langevin Monte Carlo depends critically on the condition number of the Hessian of the log-density (Durmus and Moulines, 2017; Vempala and Wibisono, 2019; Chewi et al., 2025). When the geometry of the state space is highly anisotropic, the vanilla Langevin diffusion can mix slowly along ill-conditioned directions. Consequently, appropriate preconditioning can substantially improve the convergence of the Langevin Monte Carlo (4.6) used for velocity estimation (Girolami and Calderhead, 2011; Patterson and Teh, 2013).
- (ii) For non-log-concave target distributions, appropriate preconditioning is essential for efficient exploration of the state space. Given the close connection between sampling and optimization, and the long-standing recognition of preconditioning as a key component in non-convex optimization, for example in neural network training (Amari, 1998; Martens, 2010; Duchi et al., 2011; Kingma and Ba, 2015; Dahmen et al., 2025), it is natural to expect preconditioning to play an equally important role in non-log-concave sampling. In particular, suitable preconditioning can substantially improve the convergence of the Langevin Monte Carlo (4.6) used for initialization.

Therefore, we introduce preconditioning into the Langevin algorithms used for velocity estimation (4.2) and for initialization (5.1). Before proceeding, we recall the Langevin diffusion with invariant distribution  $\pi \in C^2(\mathbb{R}^d)$ :

$$(6.1) \quad d\tilde{\theta}_t = \nabla \log \pi(\tilde{\theta}_t) dt + \sqrt{2} dB_t, \quad t \geq 0.$$

The preconditioned Langevin diffusion is defined as

$$(6.2) \quad d\theta_t = \underbrace{P(\theta_t) \nabla \log \pi(\theta_t) dt}_{\text{preconditioned score}} + \underbrace{\text{div } P(\theta_t) dt}_{\text{correction}} + \underbrace{\sqrt{2P(\theta_t)} dB_t}_{\text{preconditioned noise}}, \quad t \geq 0,$$

where  $P(\theta_t) \succeq 0$  is a probably state-dependent preconditioner, and  $\text{div}$  denotes the row-wise divergence of a matrix-valued function, that is,  $(\text{div } P(\theta_t))_k = \sum_{\ell=1}^d \partial_\ell P_{k\ell}(\theta_t)$ . If  $P(\theta) \equiv P$  is a state-independent preconditioner, then the correction term vanishes. In particular, if  $P(\theta) \equiv I_d$ , the preconditioned Langevin diffusion degenerates to the vanilla Langevin diffusion (6.1).

*Remark 6.1* (Comparison with preconditioned optimization). In preconditioned gradient flow, the preconditioner modifies only the gradient of the objective function. In contrast, the preconditioned Langevin diffusion (6.2) alters not only the gradient (drift) term but also the noise term, and additionally introduces a correction term.

This correction term in (6.2) is essential to ensure that the invariant distribution of the preconditioned Langevin diffusion coincides with that of the vanilla Langevin diffusion (6.1), as established in the following proposition, see also Ma et al. (2015, Theorem 1).

**Proposition 6.2** (Invariant distribution of preconditioned Langevin diffusion). *Suppose that  $\pi \in C^2(\mathbb{R}^d)$ . Assume further  $P(\theta) \succeq 0$  for each  $\theta \in \mathbb{R}^d$ . Then the invariant distribution of the preconditioned Langevin diffusion (6.2) is the same as that of the vanilla Langevin diffusion (6.1).*

For the convenience of the reader, a proof of Proposition 6.2 is provided in the appendix.

In this work, we adopt the RMSprop-based preconditioning strategy proposed by [Li et al. \(2016\)](#) for Langevin diffusion. This approach is Hessian-free and circumvents the computational burden of matrix inversion. The diagonal preconditioner  $P(\theta_t)$  is defined as:

$$P(\theta_t) = \text{diag}\left(\frac{1}{\sqrt{v(\theta_t)} + \epsilon}\right),$$

$$\frac{dv(\theta_t)}{dt} = (1 - \alpha)(\nabla \log \pi(\theta_t) \odot \nabla \log \pi(\theta_t) - v(\theta_t)),$$

where the second equality is known as accumulator dynamics, which describes an exponential moving average of squared score in continuous time. Here  $\epsilon > 0$  is the precision tolerance for numerical stability,  $\alpha \in (0, 1)$  is the smoothing parameter for exponential moving average, and the notation  $\odot$  denotes the entry-wise multiplication of two vectors.

*Remark 6.3.* [Li et al. \(2016, Corollary 2\)](#) shows that, when RMSprop-based preconditioning is used, the effect of the correction term  $\text{div } P(\theta_t)$  in (6.2) becomes negligible provided that the smoothing parameter  $\alpha$  is close to 1. Consequently, this term is typically omitted in practical implementations.

RMSprop-based preconditioning is effective for both velocity estimation and initialization for the following reasons:

- (i) **Velocity estimation.** In Langevin Monte Carlo used for velocity estimation, the target distribution is log-concave. An RMSprop-based preconditioner can reduce the effective condition number by approximating the diagonal of the inverse Hessian ([Dauphin et al., 2015; Li et al., 2016](#)). Intuitively, RMSprop-based preconditioning induces adaptive step sizes that reflect the local geometry of the target distribution: it assigns smaller step sizes to steep directions (characterized by large squared gradients) and larger step sizes to flatter directions (characterized by small squared gradients). This adaptive behavior is more efficient than using a fixed step size in standard Langevin dynamics.
- (ii) **Initialization.** During the initialization phase, although the starting distribution  $p_{X_{T_0}}$  is generally more tractable than the final target, it may typically exhibit multi-modality. In this context, RMSprop-based preconditioning is crucial for facilitating transitions between distinct modes. The regions separating these modes (energy barriers) are often characterized by saddle points or plateaus where the energy landscape is flat, resulting in vanishing gradients ([Dauphin et al., 2014](#)). Under vanilla Langevin diffusion, the sampler struggles to traverse these low-gradient regions due to the coupling of the step size with the gradient magnitude. In contrast, preconditioned Langevin diffusion rescales the dynamics by the inverse of the gradient magnitude; this effectively amplifies the step size and stochastic noise in flat directions, thereby enhancing exploration and significantly improving the capability to escape saddle points ([Dauphin et al., 2014; Li et al., 2016; Zhou et al., 2024](#)).

The preconditioned counterparts of velocity estimation (Algorithm 1) and initialization (Algorithm 2) are provided in Appendix D.

## 7 Numerical Experiments

In this work, we conduct a series of numerical experiments to demonstrate the efficiency of SSI. In Section 7.1, we investigate two-dimensional examples, while Section 7.2 extends

this analysis to high-dimensional settings. In Section 7.3, we explore applications in Bayesian inference. Finally, in Section 7.4, we provide ablation studies showing the influence of initialization time and the benefits of preconditioning introduced in Section 6.

**7.1 Two-dimensional distributions.** This subsection compares SSI with different baselines in two-dimensional distributions. The proposed SSI demonstrates superior performance in capturing complex, multi-modal distributions, consistently achieving the best results in distributional metrics.

**Baselines.** We benchmark our method against several well-established algorithms: unadjusted Langevin algorithm (ULA), Metropolis-adjusted Langevin algorithm (MALA), preconditioned ULA (pULA) in Section 6, and Hamiltonian Monte Carlo (HMC) (Hoffman and Gelman, 2014). For all baselines, we employ initialization from either a standard Gaussian distribution or the original point. Detailed hyperparameters for these methods are summarized in Appendix E.

**Target distributions.** We evaluate our method and baselines on three challenging two-dimensional distributions: the `rings` distribution (Grenioux et al., 2024), a mixture of  $7 \times 7$  Gaussian grid (MoG7x7), and a random mixture of 40 Gaussians (MoG40) (Midgley et al., 2023). These distributions are visualized in the left-top panel of Figures 2, 3, and 4, respectively.

**Experimental results.** The quantitative results for the different sampling methods across various metrics are summarized in Table 1. To provide a visual comparison, the sampling results for the `rings`, MoG7x7, and MoG40 distributions are illustrated in Figures 2, 3, and 4, respectively.

Table 1: Comparison of negative log likelihood (NLL), maximum mean discrepancy (MMD), and 2-Wasserstein distance ( $\mathcal{W}_2$ ) for different sampling methods.

	Metric	ULA	MALA	pULA	HMC	SSI (ours)
<code>rings</code>	NLL ↓	$1.43 \times 10^2$	$3.85 \times 10^1$	$1.05 \times 10^1$	<b>5.64</b>	8.26
	MMD ↓	$1.92 \times 10^{-2}$	$3.59 \times 10^{-2}$	$2.48 \times 10^{-2}$	$7.79 \times 10^{-3}$	<b><math>3.24 \times 10^{-3}</math></b>
	$\mathcal{W}_2$ ↓	<b>1.72</b>	5.45	4.83	1.89	2.05
MoG7x7	NLL ↓	5.61	<b>4.86</b>	5.45	8.12	5.35
	MMD ↓	2.21	3.08	$4.28 \times 10^{-2}$	1.23	<b><math>1.10 \times 10^{-3}</math></b>
	$\mathcal{W}_2$ ↓	$2.58 \times 10^1$	$2.62 \times 10^1$	9.04	$2.51 \times 10^1$	<b><math>9.73 \times 10^{-1}</math></b>
MoG40	NLL ↓	7.10	<b>6.55</b>	7.16	6.95	6.96
	MMD ↓	$4.08 \times 10^{-2}$	$4.34 \times 10^{-1}$	$2.72 \times 10^{-2}$	$2.69 \times 10^{-2}$	<b><math>2.04 \times 10^{-3}</math></b>
	$\mathcal{W}_2$ ↓	$1.82 \times 10^1$	$2.71 \times 10^1$	$1.66 \times 10^1$	$1.32 \times 10^1$	<b>3.85</b>
Many Well	NLL ↓	$4.44 \times 10^2$	$1.25 \times 10^2$	8.55	$3.12 \times 10^1$	<b>8.40</b>

Table 1 quantitatively compares the performance of SSI against baseline methods across four benchmark distributions. SSI achieves the lowest Maximum Mean Discrepancy (MMD) across all three two-dimensional target distributions. Notably, in the MoG7x7 and MoG40 experiments, SSI outperforms the baselines by orders of magnitude. This indicates that SSI captures the detailed structure of the target distributions significantly better than competing methods. In the challenging multi-modal Gaussian mixture tasks (MoG7x7 and MoG40), SSI achieves the lowest 2-Wasserstein distance by a large margin. This confirms that SSI successfully overcomes the energy barriers between modes that trap other methods.

*Remark 7.1* (Advantages of pULA over ULA). Comparing pULA with the vanilla ULA highlights the benefits of the preconditioning strategy employed in pULA. pULA consistently

outperforms ULA in the multi-modal Mixture of Gaussians experiments: MoG7x7 and MoG40. This suggests that the RMSprop preconditioner helps the sampler traverse the low-density regions between modes more effectively than ULA.

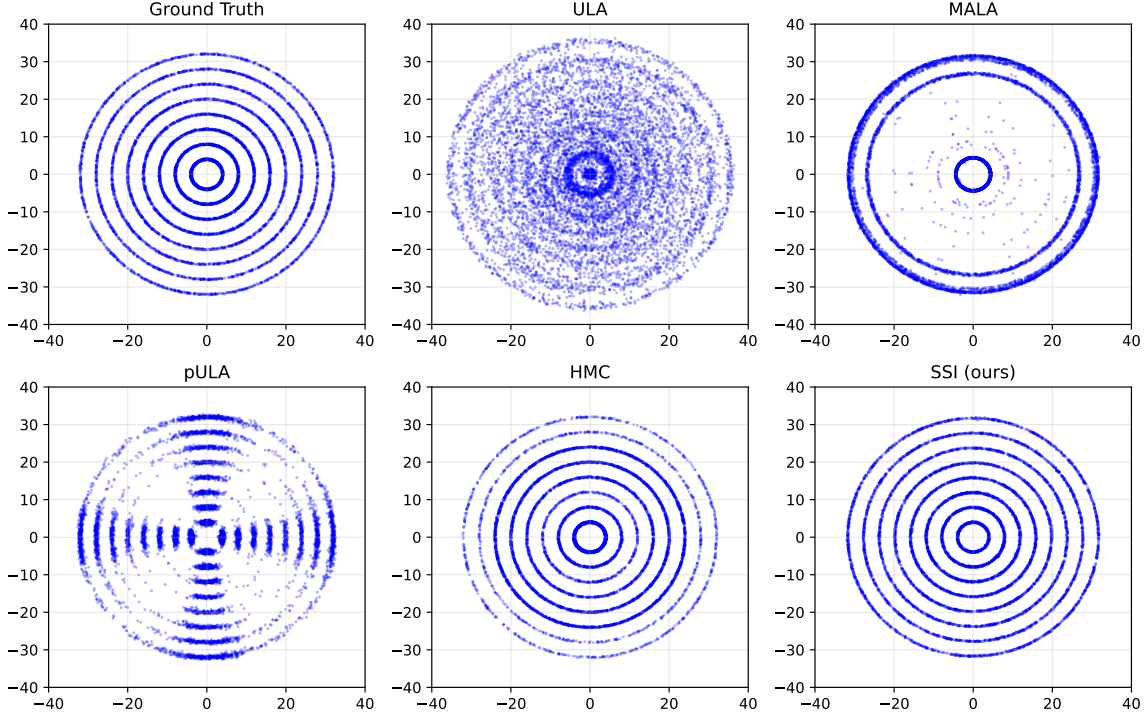


Figure 2: Comparison of SSI against baseline methods for the `rings` distribution in Section 7.1. The blue points represent  $10^4$  particles generated by each method.

The results for the `rings` distribution are presented in Figure 2. To enable ULA to capture all rings of the target distribution, we employed a large step size to enhance its exploratory capability. However, this large step size prevents ULA from capturing the local detailed features of the target distribution. In contrast, due to its rejection procedure and adaptive step size, MALA successfully captures the local detailed structure; nevertheless, it is only able to identify three of the eight rings. Similarly, pULA exhibits an adaptive step size that allows it to resolve local geometry. As discussed in Section 6, while preconditioning generally improves exploration, the anisotropy of the RMSprop preconditioner causes pULA to capture structure primarily along the axes. HMC not only captures all eight rings but also adapts to the local geometry. However, by the construction of the `rings` distribution, each ring carries equal probability mass. Consequently, particles should appear sparser on the outer rings and denser on the inner rings. The particles sampled by HMC do not adhere to this distribution property. In contrast, our proposed SSI not only accurately captures all rings but also correctly recovers the relative weights of the different rings.

The results for the MoG7x7 distribution are displayed in Figure 3. The particles sampled by ULA, MALA, and HMC remain concentrated around the initialization region. This limitation arises because these methods are unable to traverse the high energy barriers separating the modes. In the case of pULA, the RMSprop preconditioner induces larger step sizes and significant noise perturbations in the low-density regions between distinct modes, thereby

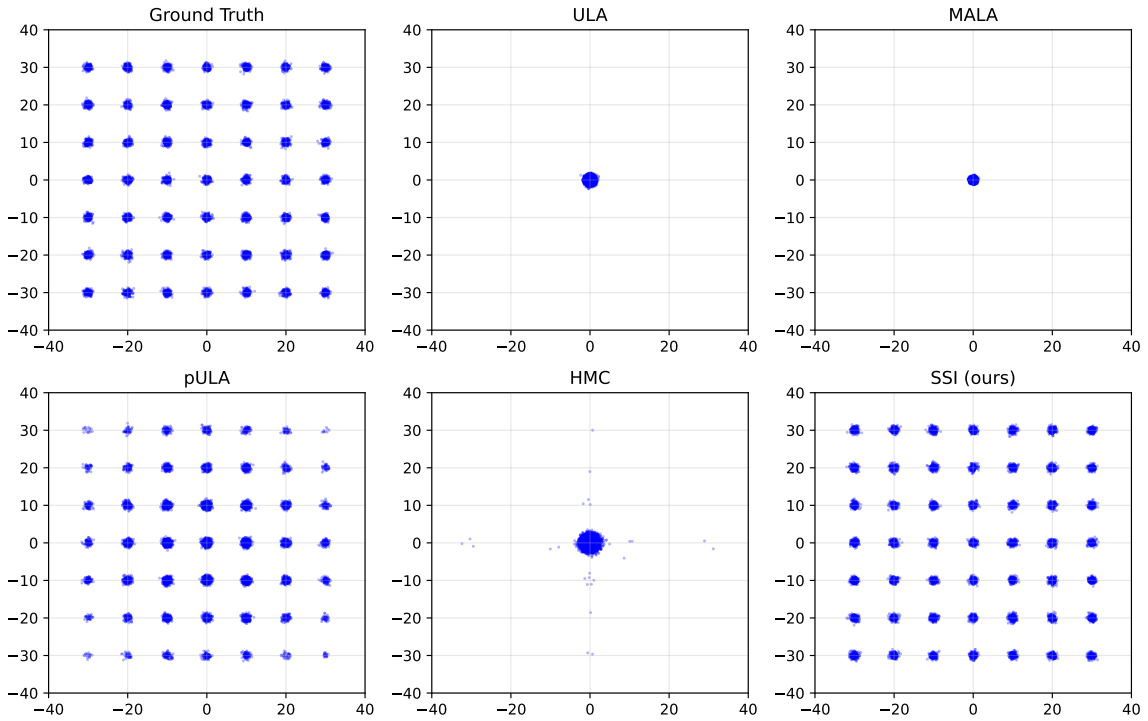


Figure 3: Comparison of SSI against baseline methods for the MoG7x7 distribution in Section 7.1. The blue points represent  $10^4$  particles generated by each method.

facilitating exploration. However, pULA fails to correctly recover the relative weights of the different modes, as evidenced by the insufficient number of particles in the outer modes. In contrast, SSI not only captures all modes of the Gaussian mixture but also accurately recovers their relative weights.

The results for the MoG40 distribution are presented in Figure 4. None of the baseline methods are able to capture all 40 modes of the target distribution. In contrast, SSI successfully captures all modes and accurately recovers their relative weights.

**7.2 High-Dimensional Distributions.** In this subsection, we demonstrate the efficacy of SSI on high-dimensional distributions. We consider the `Many Well` distribution (Midgley et al., 2023) as a representative example, which is characterized by its highly multi-modal nature.

Table 1 indicates that SSI achieves the lowest Negative Log Likelihood (NLL) compared to the baseline methods, demonstrating its efficiency in locating high-probability regions within complex energy landscapes. Figure 5 provides a visualization of these results, showing that SSI successfully captures all modes of the `Many Well` distribution.

**7.3 Bayesian inference.** In this subsection, we investigate the efficacy of SSI in the context of Bayesian inference (Lee et al., 2010; Heng et al., 2021; Durmus and Moulines, 2019). We specifically consider the inference of cluster centers in a one-dimensional Gaussian mixture model (Lee et al., 2010; Heng et al., 2021). Let  $Y_{1:m} = \{Y_i\}_{i=1}^m$  denote a set of independent and identically distributed observations drawn from a one-dimensional Gaussian

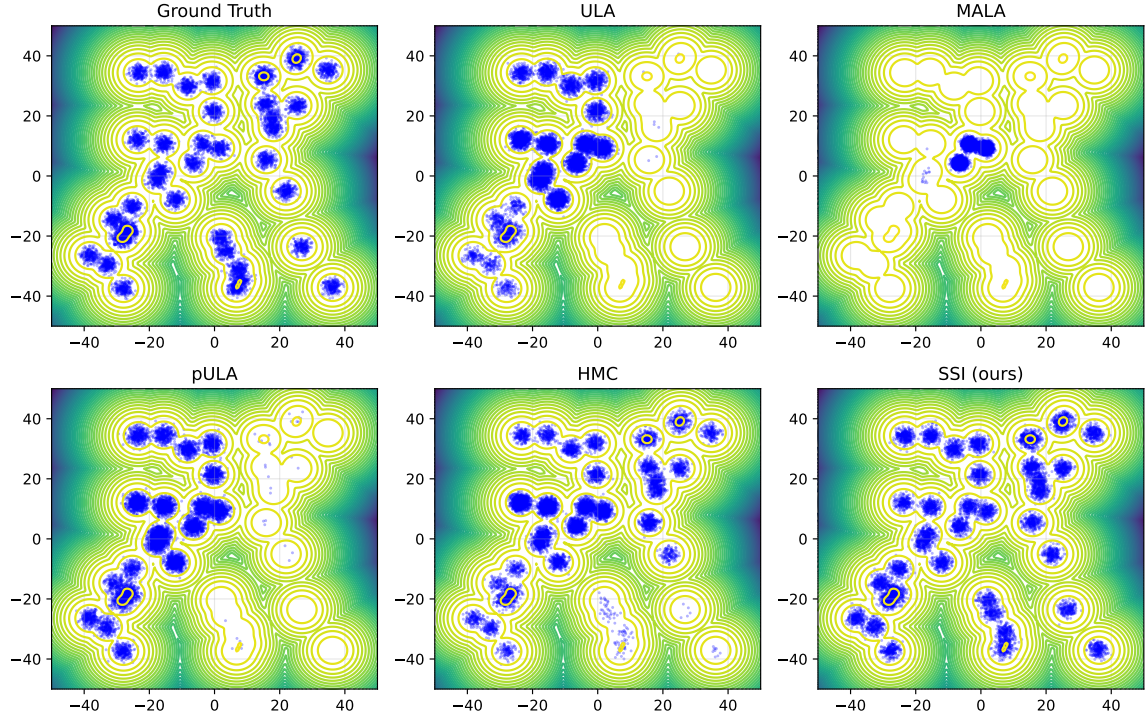


Figure 4: Comparison of SSI against baseline methods for the MoG40 distribution in Section 7.1. The blue points represent  $10^4$  particles generated by each method.

mixture with a known common variance  $\sigma^2$ :

$$Y_1, \dots, Y_m \sim \text{i.i.d. } \frac{1}{K} \sum_{k=1}^K N(\theta_k, \sigma^2),$$

where the vector of centers  $\theta_{1:K} = (\theta_1, \dots, \theta_K)^\top$  represents the unknown parameters to be estimated. By assuming a uniform prior over the parameter vector  $\theta_{1:K}$ , we obtain the following unnormalized posterior density given the measurements  $Y_{1:m}$ :

$$(7.1) \quad p(\theta_{1:K} | Y_{1:m}) \propto \underbrace{\prod_{i=1}^m \left\{ \frac{1}{K} \sum_{k=1}^K \gamma_{\sigma^2}(Y_i - \theta_k) \right\}}_{\text{likelihood}} \underbrace{\prod_{k=1}^K \text{unif}_{[a,b]}(\theta_k)}_{\text{prior}}.$$

The goal of Bayesian inference is to sample from the posterior distribution defined in (7.1). The experimental results obtained using SSI are illustrated in Figure 6.

**Multi-modality of the posterior.** As highlighted by Heng et al. (2021, Section 5.1), the posterior distribution in (7.1) is invariant under any permutation of the parameter vector  $\theta_{1:K}$ . Specifically, for any permutation matrix  $Q \in \mathbb{R}^{K \times K}$ , the following holds:

$$p(\theta_{1:K} | Y_{1:m}) = p(Q\theta_{1:K} | Y_{1:m}), \quad \theta_{1:K} \in \mathbb{R}^K.$$

This permutation invariance implies that if the posterior  $p(\cdot | Y_{1:m})$  possesses a mode centered at  $\theta_{1:K}^* \in \mathbb{R}^K$ , where each element  $\theta_k^*$  is distinct (i.e.,  $\theta_\ell^* \neq \theta_k^*$  for all  $\ell \neq k$ ), then there exist

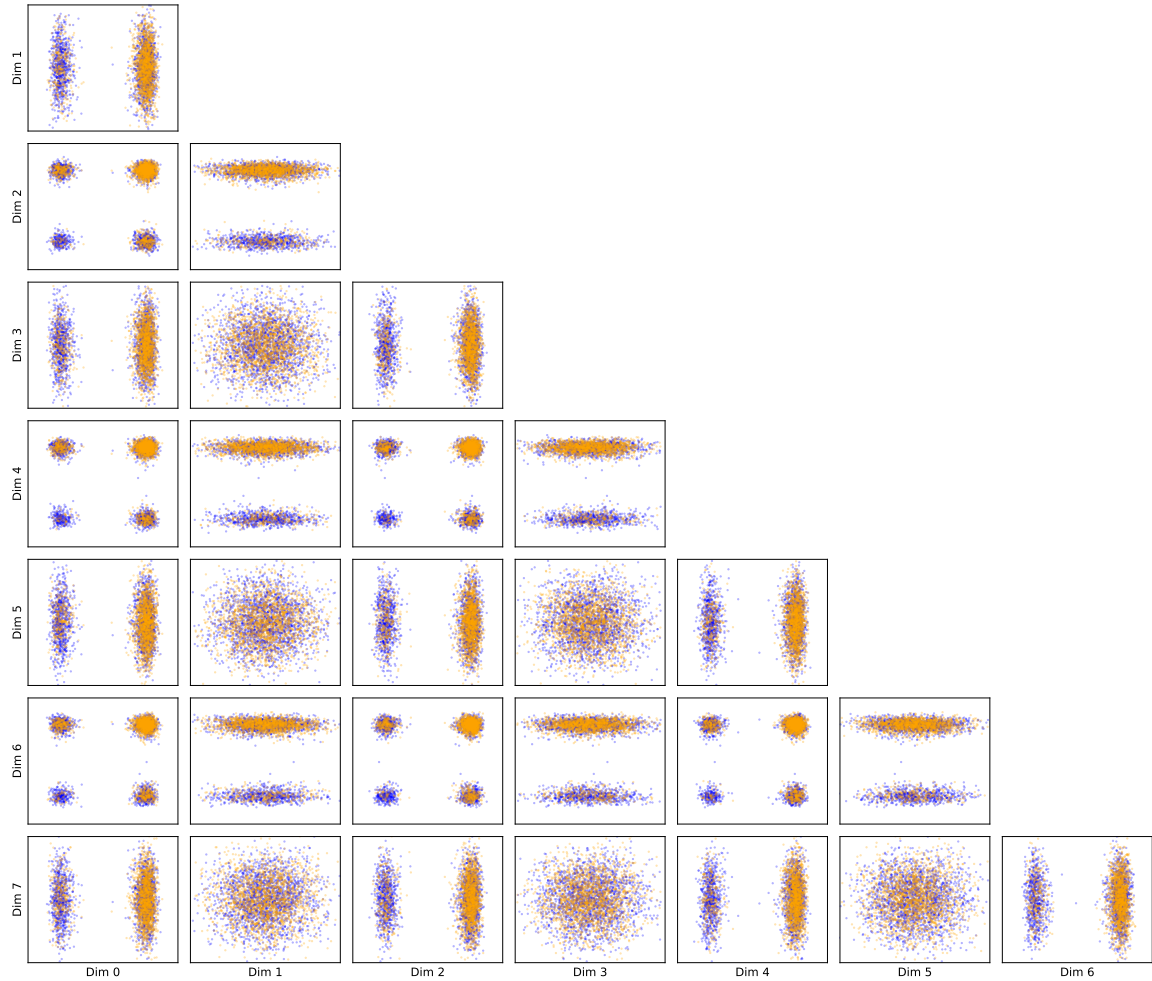


Figure 5: Pairwise marginal distributions on  $\mathbb{R}^2$  for the Many Well distribution. The orange points represent samples from the ground truth distribution, while the blue points represent the particles generated by SSI.

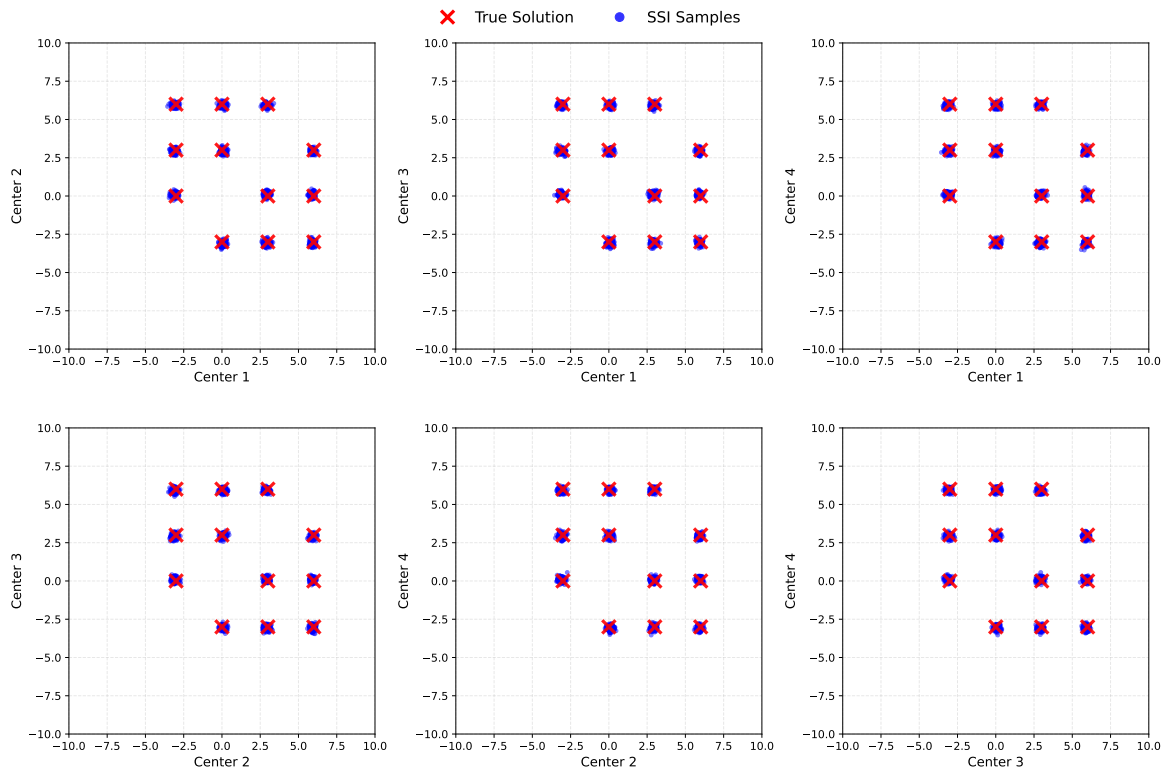


Figure 6: Pairwise marginal posterior distributions on  $\mathbb{R}^2$  for the Bayesian Gaussian model in Section 7.3. The red crosses indicate the true locations of the posterior modes, while the blue points represent the particles sampled by SSI.

$(K! - 1)$  additional distinct modes. These modes correspond to all possible permutations of  $\theta_{1:K}^*$ , depicted as red crosses in Figure 6. Such a multi-modal structure poses significant challenges for conventional sampling algorithms.

**Experimental results on Bayesian mixture models.** In this experiment, we consider a mixture of four one-dimensional Gaussians with centers located at  $\{-3, 0, 3, 6\}$ . The prior is chosen as a uniform distribution on  $(-10, 10)^4$ . Consequently, all permutations of  $\theta_{1:4}^* = (-3, 0, 3, 6)$  represent valid modes of the posterior. The particles generated by SSI are shown as blue points in Figure 6. These results demonstrate that SSI successfully captures all  $4! = 24$  modes of the posterior distribution (7.1).

**7.4 Ablation studies.** In this subsection, we provide an ablation study to show the influence of the choice of the initialization time  $T_0$  in (3.6), and demonstrate the benefits of preconditioning introduced in Section 6. We take MoG7x7 as an example. The MMD and  $\mathcal{W}_2$  change against the initialization time  $T_0$  are shown in Figure 7.

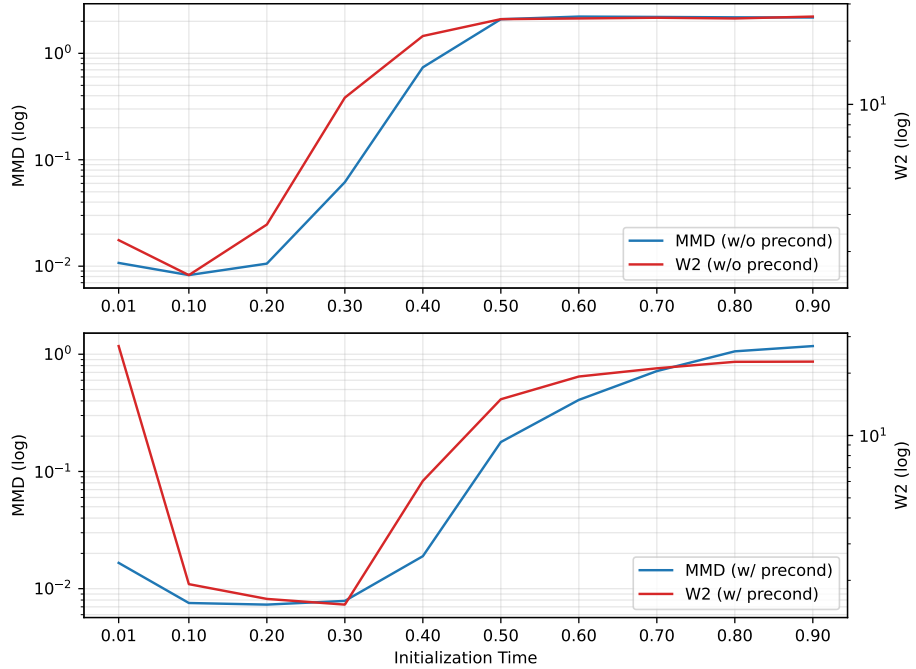


Figure 7: Results of the ablation studies on MoG7x7 in Section 7.4. **(top)** MMD and  $\mathcal{W}_2$  of SSI without preconditioning as a function of initialization time. **(bottom)** MMD and  $\mathcal{W}_2$  of SSI with preconditioning as a function of initialization time.

**The choice of the initialization time.** As shown in Figure 7, the performance of SSI, both with and without preconditioning, is non-monotonic with respect to the initialization time. Specifically, errors are large for both small initialization times and times approaching one. This empirical observation aligns with our theoretical results in Propositions 4.1 and 5.1. For sufficiently small initialization times, the convergence of the Langevin diffusion (4.2) for velocity estimation cannot be guaranteed (Proposition 4.1), leading to significant errors. Conversely, for sufficiently large initialization times, the initialization distribution  $p_{X_{T_0}}$  is close to the target distribution  $p_{X_1}$ ; it becomes highly multi-modal, preventing the Langevin diffusion (5.1) from converging rapidly during initialization (Proposition 5.1).

**The benefits of preconditioning.** Figure 7 demonstrates that SSI with preconditioning outperforms the method without preconditioning for nearly every choice of initialization time, highlighting the advantages of the technique introduced in Section 6. More importantly, the top panel of Figure 7 reveals that SSI without preconditioning is highly sensitive to the initialization time, yielding acceptable performance only at  $T_0 = 0.1$ . In contrast, SSI with preconditioning exhibits a broader “sweet spot,” ranging from  $T_0 = 0.1$  to  $T_0 = 0.3$ . This demonstrates that preconditioning significantly enhances robustness to the choice of initialization time. Furthermore, enabling the use of a larger initialization time reduces the number of iterations required to simulate the probability flow ODE (5.5), thereby lowering computational costs. This improvement arises because preconditioning simultaneously improves the sampling performance of Langevin diffusion for both velocity estimation and initialization. These results further highlight the advantages of our preconditioned approach over existing methods based on vanilla Langevin diffusion, such as [Huang et al. \(2024a\)](#); [Grenioux et al. \(2024\)](#).

**The necessity of Langevin-based initialization.** For the initialization time  $T_0 = 0.01$ , Langevin-based initialization becomes unnecessary, and a simple Gaussian initialization suffices, since the initialization distribution  $p_{X_{T_0}}$  remains close to the standard Gaussian. However, as shown in Figure 7, while choosing a small initialization time eliminates the need for this Langevin-based initialization step, it leads to a non-negligible accuracy loss in both the preconditioned and non-preconditioned cases. These experiments demonstrate that our method significantly outperforms other diffusion-based samplers that utilize Langevin-based velocity estimation and Gaussian initialization.

## 8 Conclusions

We propose a novel framework for sampling from unnormalized Boltzmann densities driven by linear stochastic interpolants. Linear stochastic interpolants induce a probability flow ODE that transports an initialization distribution to the target distribution. The initialization distribution is given by a Gaussian convolution of the target density and is therefore substantially easier to sample from. Moreover, by Tweedie’s formula, the velocity field of the probability flow ODE can be estimated via Monte Carlo methods, where the associated sampling distribution is likewise significantly simpler. As a result, our approach decomposes the challenging problem of sampling from a multi-modal and complex target density into a sequence of tractable subproblems, each of which can be addressed using Langevin diffusion. These sub-sampling tasks include (i) using Langevin diffusion to generate samples from the initialization distribution, and (ii) employing Langevin diffusion to estimate the velocity field. Simulating the resulting probability flow ODE with Langevin-based initialization and velocity estimation yields samples distributed according to the target density.

Extensive numerical experiments validate the efficiency and robustness of the proposed SSI framework. On a diverse suite of two-dimensional benchmarks, SSI consistently outperforms established baselines, including ULA, MALA, pULA, and HMC. Visualizations demonstrate that SSI effectively overcomes high energy barriers to accurately capture complex multi-modal structures and recover relative weights, whereas baseline methods often suffer from mode collapse or fail to traverse low-density regions. We further demonstrated the scalability of SSI to high-dimensional settings and its applicability to Bayesian inference, where it successfully recovered the highly multi-modal posterior distributions of mixture models. Finally, our ablation studies empirically confirmed the theoretical trade-offs regarding the initialization

time and highlighted the critical importance of preconditioning. The proposed preconditioning strategy was shown to significantly enhance the robustness of the sampler to hyperparameter choices and improve convergence in complex multi-modal landscapes.

## References

Tara Akhoun-Sadegh, Jarrid Rector-Brooks, Avishek Joey Bose, Sarthak Mittal, Pablo Lemos, Cheng-Hao Liu, Marcin Sendera, Siamak Ravanbakhsh, Gauthier Gidel, Yoshua Bengio, et al. Iterated denoising energy matching for sampling from boltzmann densities. In *The Eleventh International Conference on Learning Representations*, 2024. (Cited on page 33.)

Michael Albergo, Nicholas M. Boffi, and Eric Vanden-Eijnden. Stochastic interpolants: A unifying framework for flows and diffusions. *Journal of Machine Learning Research*, 26(209):1–80, 2025. (Cited on pages 2 and 5.)

Michael Samuel Albergo and Eric Vanden-Eijnden. Building normalizing flows with stochastic interpolants. In *The Eleventh International Conference on Learning Representations*, 2023. (Cited on pages 2 and 5.)

Shun-ichi Amari. Natural gradient works efficiently in learning. *Neural Computation*, 10(2):251–276, 1998. (Cited on page 13.)

Luigi Ambrosio, Nicola Gigli, and Giuseppe Savaré. *Gradient flows: in metric spaces and in the space of probability measures*. Springer Science & Business Media, 2005. (Cited on page 5.)

Michael Arbel, Alex Matthews, and Arnaud Doucet. Annealed flow transport monte carlo. In *Proceedings of the 38th International Conference on Machine Learning*, volume 139 of *Proceedings of Machine Learning Research*, pages 318–330. PMLR, 18–24 Jul 2021. (Cited on page 3.)

Dominique Bakry and Michael Émery. Diffusions hypercontractives. In Jacques Azéma and Marc Yor, editors, *Séminaire de Probabilités XIX 1983/84*, pages 177–206. Springer Berlin Heidelberg, 1985. (Cited on page 4.)

J. Berner, L. Richter, and K. Ullrich. An optimal control perspective on diffusion-based generative modeling. *Transactions on Machine Learning Research*, 2024. ISSN 2835-8856. URL <https://openreview.net/forum?id=oYIjw37pTP>. (Cited on page 3.)

Eliot Beyler and Francis Bach. Convergence of deterministic and stochastic diffusion-model samplers: A simple analysis in Wasserstein distance, 2025. arXiv:2508.03210. (Cited on page 7.)

Jinyuan Chang, Chenguang Duan, Yuling Jiao, Ruoxuan Li, Jerry Zhijian Yang, and Cheng Yuan. Provable diffusion posterior sampling for Bayesian inversion, 2025. arXiv:2512.08022. (Cited on page 1.)

Jannis Chemeddine, Christian Wald, Richard Duong, and Gabriele Steidl. Neural sampling from Boltzmann densities: Fisher-Rao curves in the Wasserstein geometry. In *The Thirteenth International Conference on Learning Representations*, 2025. (Cited on pages 2 and 3.)

Hong-Bin Chen, Sinho Chewi, and Jonathan Niles-Weed. Dimension-free log-Sobolev inequalities for mixture distributions. *Journal of Functional Analysis*, 281(11):109236, 2021. ISSN 0022-1236. (Cited on page 7.)

Wenlin Chen, Mingtian Zhang, Brooks Paige, José Miguel Hernández-Lobato, and David Barber. Diffusive Gibbs sampling. In Ruslan Salakhutdinov, Zico Kolter, Katherine Heller, Adrian Weller, Nuria Oliver, Jonathan Scarlett, and Felix Berkenkamp, editors, *Proceedings of the 41st International Conference on Machine Learning*, volume 235 of *Proceedings of Machine Learning Research*, pages 7731–7747. PMLR, 21–27 Jul 2024. (Cited on page 2.)

Sinho Chewi, Murat A. Erdogdu, Mufan Li, Ruoqi Shen, and Matthew S. Zhang. Analysis of Langevin Monte Carlo from Poincaré to Log-Sobolev. *Foundations of Computational Mathematics*, 25:1345–1395, 2025. (Cited on pages 4 and 13.)

Hyungjin Chung, Jeongsol Kim, Michael Thompson Mccann, Marc Louis Klasky, and Jong Chul Ye. Diffusion posterior sampling for general noisy inverse problems. In *The Eleventh International Conference on Learning Representations*, 2023. (Cited on page 1.)

Adam D. Cobb and Brian Jalaian. Scaling hamiltonian monte carlo inference for bayesian neural networks with symmetric splitting. In Cassio de Campos and Marloes H. Maathuis, editors, *Proceedings of the Thirty-Seventh Conference on Uncertainty in Artificial Intelligence*, volume 161 of *Proceedings of Machine Learning Research*, pages 675–685. PMLR, 27–30 Jul 2021. (Cited on page 1.)

Wolfgang Dahmen, Wuchen Li, Yuankai Teng, and Zhu Wang. Expansive natural neural gradient flows for energy minimization, 2025. arXiv:2507.13475. (Cited on page 13.)

Giannis Daras, Alexandros G Dimakis, and Constantinos Daskalakis. Consistent diffusion meets Tweedie: Training exact ambient diffusion models with noisy data. *arXiv preprint arXiv:2404.10177*, 2024. (Cited on page 30.)

Yann Dauphin, Harm de Vries, and Yoshua Bengio. Equilibrated adaptive learning rates for non-convex optimization. In C. Cortes, N. Lawrence, D. Lee, M. Sugiyama, and R. Garnett, editors, *Advances in Neural Information Processing Systems*, volume 28. Curran Associates, Inc., 2015. (Cited on page 14.)

Yann N Dauphin, Razvan Pascanu, Caglar Gulcehre, Kyunghyun Cho, Surya Ganguli, and Yoshua Bengio. Identifying and attacking the saddle point problem in high-dimensional non-convex optimization. In Z. Ghahramani, M. Welling, C. Cortes, N. Lawrence, and K.Q. Weinberger, editors, *Advances in Neural Information Processing Systems*, volume 27. Curran Associates, Inc., 2014. (Cited on page 14.)

Zhao Ding, Chenguang Duan, Yuling Jiao, Ruoxuan Li, Jerry Zhijian Yang, and Pingwen Zhang. Characteristic learning for provable one step generation, 2024a. arXiv:2405.05512. (Cited on pages 5, 7, 12, and 32.)

Zhao Ding, Chenguang Duan, Yuling Jiao, Jerry Zhijian Yang, Cheng Yuan, and Pingwen Zhang. Nonlinear assimilation via score-based sequential Langevin sampling, 2024b. arXiv:2411.13443. (Cited on pages 1 and 2.)

Jing Dong and Xin T. Tong. Spectral gap of replica exchange Langevin diffusion on mixture distributions. *Stochastic Processes and their Applications*, 151:451–489, 2022. (Cited on page 8.)

John Duchi, Elad Hazan, and Yoram Singer. Adaptive subgradient methods for online learning and stochastic optimization. *Journal of Machine Learning Research*, 12(61):2121–2159, 2011. (Cited on page 13.)

Alain Durmus and Éric Moulines. Nonasymptotic convergence analysis for the unadjusted Langevin algorithm. *The Annals of Applied Probability*, 27(3):1551 – 1587, 2017. (Cited on page 13.)

Alain Durmus and Éric Moulines. High-dimensional Bayesian inference via the unadjusted Langevin algorithm. *Bernoulli*, 25(4A):2854–2882, 2019. (Cited on pages 1 and 17.)

Bradley Efron. Tweedie’s formula and selection bias. *Journal of the American Statistical Association*, 106(496):1602–1614, 2011. (Cited on pages 2 and 30.)

W. R. Gilks, S. Richardson, and D. Spiegelhalter. *Markov Chain Monte Carlo in Practice*. Springer, 1995. (Cited on page 1.)

Mark Girolami and Ben Calderhead. Riemann manifold Langevin and Hamiltonian Monte Carlo methods. *Journal of the Royal Statistical Society Series B: Statistical Methodology*, 73(2):123–214, 2011. (Cited on page 13.)

Louis Grenioux, Maxence Noble, Marylou Gabrié, and Alain Oliviero Durmus. Stochastic localization via iterative posterior sampling. In Ruslan Salakhutdinov, Zico Kolter, Katherine Heller, Adrian Weller, Nuria Oliver, Jonathan Scarlett, and Felix Berkenkamp, editors, *Proceedings of the 41st International Conference on Machine Learning*, volume 235 of *Proceedings of Machine Learning Research*, pages 16337–16376. PMLR, 21–27 Jul 2024. (Cited on pages 2, 7, 15, and 22.)

Wei Guo, Jaemoo Choi, Yuchen Zhu, Molei Tao, and Yongxin Chen. Proximal diffusion neural sampler, 2025a. arXiv:2510.03824. (Cited on page 3.)

Wei Guo, Molei Tao, and Yongxin Chen. Provable benefit of annealed Langevin Monte Carlo for non-log-concave sampling. In *The Thirteenth International Conference on Learning Representations*, 2025b. (Cited on pages 2 and 8.)

P. Hagemann, J. Hertrich, and G. Steidl. Stochastic normalizing flows for inverse problems: A Markov chains viewpoint. *SIAM/ASA Journal on Uncertainty Quantification*, 10(3): 1162–1190, 2022. (Cited on page 2.)

Aaron J Havens, Benjamin Kurt Miller, Bing Yan, Carles Domingo-Enrich, Anuroop Sriram, Daniel S. Levine, Brandon M Wood, Bin Hu, Brandon Amos, Brian Karrer, Xiang Fu, Guan-Horng Liu, and Ricky T. Q. Chen. Adjoint sampling: Highly scalable diffusion samplers via adjoint matching. In *Proceedings of the 42nd International Conference on Machine Learning*, volume 267 of *Proceedings of Machine Learning Research*, pages 22204–22237. PMLR, 13–19 Jul 2025. (Cited on page 3.)

Jiajun He, Wenlin Chen, Mingtian Zhang, David Barber, and José Miguel Hernández-Lobato. Training neural samplers with reverse diffusive KL divergence. In *International Conference*

on *Artificial Intelligence and Statistics*, pages 5167–5175. PMLR, 2025a. (Cited on pages 2 and 3.)

Jiajun He, Yuanqi Du, Francisco Vargas, Yuanqing Wang, Carla P. Gomes, José Miguel Hernández-Lobato, and Eric Vanden-Eijnden. FEAT: Free energy estimators with adaptive transport, 2025b. arXiv:2504.11516. (Cited on page 1.)

Ye He, Kevin Rojas, and Molei Tao. Zeroth-order sampling methods for non-log-concave distributions: Alleviating metastability by denoising diffusion, 2024. arXiv:2402.17886. (Cited on page 2.)

Jeremy Heng, Arnaud Doucet, and Yvo Pokern. Gibbs flow for approximate transport with applications to Bayesian computation. *Journal of the Royal Statistical Society Series B: Statistical Methodology*, 83(1):156–187, 2021. (Cited on pages 1, 2, 17, and 18.)

Jonathan Ho, Ajay Jain, and Pieter Abbeel. Denoising diffusion probabilistic models. In H. Larochelle, M. Ranzato, R. Hadsell, M.F. Balcan, and H. Lin, editors, *Advances in Neural Information Processing Systems*, volume 33, pages 6840–6851. Curran Associates, Inc., 2020. (Cited on page 2.)

M. D. Hoffman and A. Gelman. The No-U-turn sampler: Adaptively setting path lengths in Hamiltonian Monte Carlo. *Journal of Machine Learning Research*, 15:1593–1623, 2014. (Cited on pages 1 and 15.)

Jian Huang, Yuling Jiao, Lican Kang, Xu Liao, Jin Liu, and Yanyan Liu. Schrödinger-Föllmer sampler. *IEEE Transactions on Information Theory*, 71(2):1283–1299, 2025. (Cited on page 2.)

Xunpeng Huang, Hanze Dong, Yifan HAO, Yian Ma, and Tong Zhang. Reverse diffusion Monte Carlo. In *The Twelfth International Conference on Learning Representations*, 2024a. (Cited on pages 2 and 22.)

Xunpeng Huang, Difan Zou, Hanze Dong, Yi-An Ma, and Tong Zhang. Faster sampling without isoperimetry via diffusion-based Monte Carlo. In Shipra Agrawal and Aaron Roth, editors, *Proceedings of Thirty Seventh Conference on Learning Theory*, volume 247 of *Proceedings of Machine Learning Research*, pages 2438–2493. PMLR, 2024b. (Cited on page 2.)

Pavel Izmailov, Sharad Vikram, Matthew D Hoffman, and Andrew Gordon Gordon Wilson. What are bayesian neural network posteriors really like? In Marina Meila and Tong Zhang, editors, *Proceedings of the 38th International Conference on Machine Learning*, volume 139 of *Proceedings of Machine Learning Research*, pages 4629–4640. PMLR, 18–24 Jul 2021. (Cited on page 1.)

Diederik P. Kingma and Jimmy Ba. Adam: A method for stochastic optimization. In *International Conference on Learning Representations*, 2015. (Cited on page 13.)

David P. Landau and Kurt Binder. *A Guide to Monte Carlo Simulations in Statistical Physics*. Cambridge University Press, 4 edition, 2014. (Cited on page 1.)

Anthony Lee, Christopher Yau, Michael B. Giles, Arnaud Doucet, and Christopher C. Holmes. On the utility of graphics cards to perform massively parallel simulation of advanced Monte

Carlo methods. *Journal of Computational and Graphical Statistics*, 19(4):769–789, 2010. (Cited on page 17.)

Yin Tat Lee, Ruoqi Shen, and Kevin Tian. Structured logconcave sampling with a restricted Gaussian oracle. In Mikhail Belkin and Samory Kpotufe, editors, *Proceedings of Thirty Fourth Conference on Learning Theory*, volume 134 of *Proceedings of Machine Learning Research*, pages 2993–3050. PMLR, 15–19 Aug 2021. (Cited on page 8.)

Chunyuan Li, Changyou Chen, David Carlson, and Lawrence Carin. Preconditioned stochastic gradient Langevin dynamics for deep neural networks. In *Proceedings of the Thirtieth AAAI Conference On Artificial Intelligence*, 2016. (Cited on page 14.)

Yaron Lipman, Ricky T. Q. Chen, Heli Ben-Hamu, Maximilian Nickel, and Matthew Le. Flow matching for generative modeling. In *The Eleventh International Conference on Learning Representations*, 2023. (Cited on page 2.)

Guan-Horng Liu, Jaemoo Choi, Yongxin Chen, Benjamin Kurt Miller, and Ricky T. Q. Chen. Adjoint Schrödinger bridge sampler. In *The Thirty-ninth Annual Conference on Neural Information Processing Systems*, 2025. (Cited on page 3.)

Xingchao Liu, Chengyue Gong, and Qiang Liu. Flow straight and fast: Learning to generate and transfer data with rectified flow. In *The Eleventh International Conference on Learning Representations*, 2023. (Cited on page 5.)

Yi-An Ma, Tianqi Chen, and Emily Fox. A complete recipe for stochastic gradient mcmc. *Advances in neural information processing systems*, 28, 2015. (Cited on page 13.)

James Martens. Deep learning via Hessian-free optimization. In *Proceedings of the 27th International Conference on International Conference on Machine Learning*, pages 735–742, 2010. (Cited on page 13.)

Ségolène Tiffany Martin, Anne Gagneux, Paul Hagemann, and Gabriele Steidl. PnP-Flow: Plug-and-play image restoration with flow matching. In *The Thirteenth International Conference on Learning Representations*, 2025. (Cited on page 1.)

Bálint Máté and François Fleuret. Learning interpolations between Boltzmann densities. *Transactions on Machine Learning Research*, 2023. ISSN 2835-8856. (Cited on pages 2, 3, and 37.)

Laurence Illing Midgley, Vincent Stimper, Gregor N. C. Simm, Bernhard Schölkopf, and José Miguel Hernández-Lobato. Flow annealed importance sampling bootstrap. In *The Eleventh International Conference on Learning Representations*, 2023. (Cited on pages 1, 3, 15, and 17.)

Hossein Mobahi and John W. Fisher. On the link between Gaussian homotopy continuation and convex envelopes. In *Energy Minimization Methods in Computer Vision and Pattern Recognition*, pages 43–56, Cham, 2015. Springer International Publishing. (Cited on page 2.)

P. Del Moral, A. Doucet, and A. Jasra. Sequential Monte Carlo samplers. *Journal of the Royal Statistical Society Series B: Statistical Methodology*, 2006. (Cited on page 2.)

R. M. Neal. Annealed importance sampling. *Statistics and computing*, 11:125–139, 2001. (Cited on pages 2 and 10.)

Frank Noè, Simon Olsson, Jonas Köhler, and Hao Wu. Boltzmann generators: Sampling equilibrium states of many-body systems with deep learning. *Science*, 365(6457):eaaw1147, 2019. (Cited on page 1.)

Antony M. Overstall, David C. Woods, and Ben M. Parker. Bayesian optimal design for ordinary differential equation models with application in biological science. *Journal of the American Statistical Association*, 115(530):583–598, 2020. (Cited on page 1.)

Sam Patterson and Yee Whye Teh. Stochastic gradient Riemannian Langevin dynamics on the probability simplex. In C.J. Burges, L. Bottou, M. Welling, Z. Ghahramani, and K.Q. Weinberger, editors, *Advances in Neural Information Processing Systems*, volume 26. Curran Associates, Inc., 2013. (Cited on page 13.)

Angus Phillips, Hai-Dang Dau, Michael John Hutchinson, Valentin De Bortoli, George Deligiannidis, and Arnaud Doucet. Particle denoising diffusion sampler. In *Proceedings of the 41st International Conference on Machine Learning*, volume 235 of *Proceedings of Machine Learning Research*, pages 40688–40724. PMLR, 21–27 Jul 2024. (Cited on page 3.)

Saeed Saremi, Ji Won Park, and Francis Bach. Chain of log-concave Markov chains. In *The Twelfth International Conference on Learning Representations*, 2024. (Cited on page 7.)

Jascha Sohl-Dickstein, Eric Weiss, Niru Maheswaranathan, and Surya Ganguli. Deep unsupervised learning using nonequilibrium thermodynamics. In Francis Bach and David Blei, editors, *Proceedings of the 32nd International Conference on Machine Learning*, volume 37 of *Proceedings of Machine Learning Research*, pages 2256–2265, Lille, France, 07–09 Jul 2015. PMLR. (Cited on page 2.)

Yang Song and Stefano Ermon. Generative modeling by estimating gradients of the data distribution. In H. Wallach, H. Larochelle, A. Beygelzimer, F. d'Alché-Buc, E. Fox, and R. Garnett, editors, *Advances in Neural Information Processing Systems*, volume 32. Curran Associates, Inc., 2019. (Cited on pages 1 and 2.)

Yang Song, Jascha Sohl-Dickstein, Diederik P Kingma, Abhishek Kumar, Stefano Ermon, and Ben Poole. Score-based generative modeling through stochastic differential equations. In *International Conference on Learning Representations*, 2021. (Cited on page 2.)

Samuel Stanton, Wesley Maddox, Nate Gruver, Phillip Maffettone, Emily Delaney, Peyton Greenside, and Andrew Gordon Wilson. Accelerating Bayesian optimization for biological sequence design with denoising autoencoders. In Kamalika Chaudhuri, Stefanie Jegelka, Le Song, Csaba Szepesvari, Gang Niu, and Sivan Sabato, editors, *Proceedings of the 39th International Conference on Machine Learning*, volume 162 of *Proceedings of Machine Learning Research*, pages 20459–20478. PMLR, 17–23 Jul 2022. (Cited on page 1.)

Santosh Vempala and Andre Wibisono. Rapid convergence of the unadjusted Langevin algorithm: isoperimetry suffices. In H. Wallach, H. Larochelle, A. Beygelzimer, F. d' Alché-Buc, E. Fox, and R. Garnett, editors, *Advances in Neural Information Processing Systems*, volume 32. Curran Associates, Inc., 2019. (Cited on pages 4 and 13.)

C. Wald and G. Steidl. Flow Matching: Markov kernels, stochastic processes and transport plans. In *Variational and Information Flows in Machine Learning and Optimal Transport, Oberwolfach Seminars. Vol. 56*, pages 185–254. Birkhäuser, 2025. (Cited on pages 2 and 5.)

Yan Wang, Ling Guo, Hao Wu, and Tao Zhou. Energy-based diffusion generator for efficient sampling of Boltzmann distributions. *Neural Networks*, 194:108126, 2026. (Cited on page 3.)

Dongze Wu and Yao Xie. Annealing flow generative models towards sampling high-dimensional and multi-modal distributions. In *Forty-second International Conference on Machine Learning*, 2025. (Cited on pages 2 and 3.)

Hao Wu, Jonas Köhler, and Frank Noe. Stochastic normalizing flows. In H. Larochelle, M. Ranzato, R. Hadsell, M.F. Balcan, and H. Lin, editors, *Advances in Neural Information Processing Systems*, volume 33, pages 5933–5944. Curran Associates, Inc., 2020. (Cited on pages 2 and 3.)

Qinsheng Zhang and Yongxin Chen. Path integral sampler: A stochastic control approach for sampling. In *International Conference on Learning Representations*, 2022. (Cited on page 3.)

Yasi Zhang, Peiyu Yu, Yaxuan Zhu, Yingshan Chang, Feng Gao, Ying Nian Wu, and Oscar Leong. Flow priors for linear inverse problems via iterative corrupted trajectory matching. *arXiv preprint arXiv:2405.18816*, 2024. (Cited on page 5.)

Dongruo Zhou, Jinghui Chen, Yuan Cao, Ziyan Yang, and Quanquan Gu. On the convergence of adaptive gradient methods for nonconvex optimization. *Transactions on Machine Learning Research*, 2024. ISSN 2835-8856. Featured Certification. (Cited on page 14.)

## A Auxiliary Lemmas

For the proofs in the following section, we need some auxiliary computations.

**Lemma A.1.** *For every  $t \in (0, 1)$ , we have*

$$\nabla \mathbb{E}[X_1 | X_t = x_t] = \frac{t}{(1-t)^2} \text{Cov}(X_1 | X_t = x_t).$$

*Proof.* It follows from (4.1) that

$$\begin{aligned} \nabla \mathbb{E}[X_1 | X_t = x_t] &= \nabla \left( \int x_1 p_{X_1 | X_t = x_t}(x_1) dx_1 \right) \\ &= \nabla \left( \int x_1 \gamma_{(1-t)^2}(x_t - tx_1) \frac{p_{X_1}(x_1)}{p_{X_t}(x_t)} dx_1 \right) \\ &= - \int x_1 \left( \frac{x_t - tx_1}{(1-t)^2} \right)^\top \gamma_{(1-t)^2}(x_t - tx_1) \frac{p_{X_1}(x_1)}{p_{X_t}(x_t)} dx_1 \\ &\quad - \int x_1 \gamma_{(1-t)^2}(x_t - tx_1) \frac{p_{X_1}(x_1)}{p_{X_t}(x_t)} dx_1 \nabla \log p_{X_t}(x_t)^\top \end{aligned}$$

and further by (3.3) and (3.5) that

$$\begin{aligned} \nabla \mathbb{E}[X_1 | X_t = x_t] &= -\frac{1}{(1-t)^2} \mathbb{E}[X_1 | X_t = x_t] x_t^\top + \frac{t}{(1-t)^2} \mathbb{E}[X_1 X_1^\top | X_t = x_t] \\ &\quad + \frac{1}{(1-t)^2} \mathbb{E}[X_1 | X_t = x_t] x_t^\top - \frac{t}{(1-t)^2} \mathbb{E}[X_1 | X_t = x_t] \mathbb{E}[X_1 | X_t = x_t]^\top \\ &= \frac{t}{(1-t)^2} \text{Cov}(X_1 | X_t = x_t). \end{aligned} \quad \square$$

By similar arguments as the proof of Lemma A.1, we obtain the following lemma.

**Lemma A.2.** *Let Assumption 1 be fulfilled. Then it holds*

$$\nabla \mathbb{E}[Y|X_1 = x_1] = \frac{1}{\sigma^2} \text{Cov}(Y|X_1 = x_1).$$

Further, we will need the following relation.

**Lemma A.3.** *Let Assumption 1 be fulfilled. Then, we have for every  $t \in (0, 1)$  and  $x_t \in \mathbb{R}^d$  that*

$$(X_1|X_t = x_t) \stackrel{d}{=} \frac{t}{(1-t)^2} \sigma_t^2 x_t + \frac{\sigma_t^2}{\sigma^2} Y_t^{x_t} + \sigma_t \Xi,$$

where  $Y_t^{x_t} \sim \gamma_{\sigma^2 t^2 + (1-t)^2}(x_t - t \cdot) p_Y$  and

$$\sigma_t^2 := \frac{\sigma^2(1-t)^2}{\sigma^2 t^2 + (1-t)^2}$$

In particular, we have  $\text{supp}(Y_t^{x_t}) = \text{supp}(p_Y)$  and

$$\begin{aligned} \mathbb{E}[X_1|X_t = x_t] &= \frac{t}{(1-t)^2} \sigma_t^2 x_t + \frac{\sigma_t^2}{\sigma^2} \mathbb{E}[Y_t^{x_t}], \\ \text{Cov}(X_1|X_t = x_t) &= \frac{\sigma_t^4}{\sigma^4} \text{Cov}(Y_t^{x_t}) + \sigma_t^2 \mathbf{I}_d. \end{aligned}$$

*Proof.* By straightforward computation we obtain

$$\begin{aligned} p_{X_1|X_t=x_t}(x_1) &= \frac{1}{p_{X_t}(x_t)} \int \gamma_{(1-t)^2}(x_t - tx_1) \gamma_{\sigma^2}(x_1 - y) p_Y(y) dy \\ &= \int \gamma_{\sigma_t^2} \left( x_1 - \frac{t}{(1-t)^2} \sigma_t^2 x_t - \frac{\sigma_t^2}{\sigma^2} y \right) \gamma_{\sigma^2 t^2 + (1-t)^2}(x_t - ty) p_Y(y) dy. \end{aligned}$$

Using (2.2) yields the assertion.  $\square$

Finally, we have for  $X_1 = Y + \sigma \Xi$ , where  $Y$  is independent of  $\Xi$ , by Tweedie's formula, see, e.g. Efron (2011) or Daras et al. (2024, Lemma 3.2), that

$$(A.1) \quad \nabla \log p_{X_1}(x_1) = -\frac{1}{\sigma^2} x_1 + \frac{1}{\sigma^2} \mathbb{E}[Y|X_1 = x_1].$$

## B Proofs

**Proposition 4.1.** Let Assumption 1 be fulfilled, and let  $X_t$  be given by the linear interpolant (3.1). For  $t \in (0, 1)$  and  $\sigma^2 > 0$ , set

$$\beta_t := \frac{t^2}{(1-t)^2} + \frac{1}{\sigma^2} - \frac{R^2}{\sigma^4}.$$

Then, for every  $t \in (0, 1)$ , it holds

$$\beta_t \mathbf{I}_d \preceq -\nabla^2 \log p_{X_1|X_t=x_t} \preceq \left( \beta_t + \frac{R^2}{\sigma^4} \right) \mathbf{I}_d,$$

and  $p_{X_1|X_t=x_t}$  is  $\beta_t$ -strongly log-concave for  $t \in (T^*, 1)$ , where

$$T^* = \begin{cases} 0 & \text{if } R^2 \leq \sigma^2 \\ \frac{1}{2} & \text{if } R^2 = \sigma^2 + \sigma^4, \\ \frac{R^2 - \sigma^2 - \sigma^2 \sqrt{R^2 - \sigma^2}}{R^2 - \sigma^2 - \sigma^4} & \text{otherwise.} \end{cases}$$

We have  $T^* < \frac{1}{2}$  if  $\sigma^2 < R^2 < \sigma^2 + \sigma^4$ , and  $T^* > \frac{1}{2}$  if  $R^2 > \sigma^2 + \sigma^4$ .

Further, for  $t \in (T^*, 1)$ , it holds

$$\text{KL}\left(p_{Z_s}, p_{X_1|X_t=x_t}\right) \leq e^{-2\beta_t s} \text{KL}\left(p_{Z_0}, p_{X_1|X_t=x_t}\right).$$

where  $Z_s$ ,  $s \geq 0$  is defined by the Langevin diffusion (4.2).

*Proof.* Using (4.3), (A.1) as well as Lemma A.2, we obtain

$$\begin{aligned} \nabla^2 \log p_{X_1|X_t=x_t}(x_1) &= -\frac{t^2}{(1-t)^2} \mathbf{I}_d + \nabla^2 \log p_{X_1}(x_1) \\ &= -\frac{t^2}{(1-t)^2} \mathbf{I}_d - \frac{1}{\sigma^2} \mathbf{I}_d + \frac{1}{\sigma^2} \nabla \mathbb{E}[Y|X_1=x_1] \\ &= -\left(\beta_t + \frac{R^2}{\sigma^4}\right) \mathbf{I}_d + \frac{1}{\sigma^4} \text{Cov}(Y|X_1=x_1). \end{aligned}$$

Since  $\|Y\|_2 \leq R$  almost surely, we have

$$0 \preceq \text{Cov}(Y|X_t=x_t) \preceq R^2 \mathbf{I}_d,$$

so that

$$\beta_t \mathbf{I}_d \preceq -\nabla^2 \log p_{X_1|X_t=x_t} \preceq \left(\beta_t + \frac{R^2}{\sigma^4}\right) \mathbf{I}_d,$$

Next, we consider for  $t \in (0, 1)$  the expression

$$\begin{aligned} (1-t)^2 \sigma^4 \beta_t &= t^2 \sigma^4 + (1-t)^2 (\sigma^2 - R^2) \\ &= (\sigma^2 + \sigma^4 - R^2) t^2 - 2t(\sigma^2 - R^2) + \sigma^2 - R^2. \end{aligned}$$

If  $\sigma^2 \geq R^2$ , then clearly  $\beta_t > 0$ . If  $R^2 = \sigma^2 + \sigma^4$ , then  $\beta_t > 0$  if and only if  $t \in (\frac{1}{2}, 1)$ . Let  $\sigma^2 < R^2$ . Then the zeros of the above quadratic equation are

$$t_{\pm} = \frac{R^2 - \sigma^2 \pm \sigma^2 \sqrt{R^2 - \sigma^2}}{R^2 - \sigma^2 - \sigma^4}.$$

If  $R^2 < \sigma^2 + \sigma^4$ , then  $t_+ < 0$  and  $t_- \in (0, \frac{1}{2})$ , so that  $\beta_t > 0$  if and only if  $t \in (t_-, 1)$ . If  $R^2 > \sigma^2 + \sigma^4$ , then  $t_+ > 1$  and  $t_- \in (\frac{1}{2}, 1)$ , so that  $\beta_t > 0$  if and only if  $t \in (t_-, 1)$ . This gives  $T$  in (4.4). The final relation (4.5) follows from the  $\beta_t$ -strong log-concavity, see Theorem 2.1. This completes the proof.  $\square$

**Lemma 5.3.** Let Assumption 1 be fulfilled. For every  $t \in (0, 1)$ , it holds

$$\|u(t, x_t)\|_2 \leq B(1 + \|x_t\|_2), \quad x_t \in \mathbb{R}^d,$$

where  $B$  is a constant only depending on  $\sigma$  and  $R$ .

*Proof.* According to (3.3) and Lemma A.3, we have

$$\begin{aligned}
 u(t, x_t) &= -\frac{1}{1-t}x_t + \frac{1}{1-t}\mathbb{E}[X_1|X_t = x_t] \\
 &= -\frac{1}{1-t}x_t + \frac{1}{1-t}\frac{t}{(1-t)^2}\sigma_t^2x_t + \frac{1}{1-t}\frac{\sigma_t^2}{\sigma^2}\mathbb{E}[Y_t^{x_t}] \\
 &= \frac{\sigma^2t^2 - (1-t)}{\sigma^2t + (1-t)^2}x_t + \frac{1-t}{\sigma^2t^2 + (1-t)^2}\mathbb{E}[Y_t^{x_t}].
 \end{aligned}$$

Then using triangular inequality yields

$$\begin{aligned}
 \|u(t, x_t)\|_2 &\leq \frac{\sigma^2t^2 - (1-t)}{\sigma^2t + (1-t)^2}\|x_t\|_2 + \frac{1-t}{\sigma^2t^2 + (1-t)^2}\|\mathbb{E}[Y_t^{x_t}]\|_2 \\
 &\leq \frac{\sigma^2t^2 - (1-t)}{\sigma^2t + (1-t)^2}\|x_t\|_2 + \frac{1-t}{\sigma^2t^2 + (1-t)^2}\mathbb{E}[\|Y_t^{x_t}\|_2] \\
 &\leq \frac{\sigma^2t^2 - (1-t)}{\sigma^2t + (1-t)^2}\|x_t\|_2 + \frac{1-t}{\sigma^2t^2 + (1-t)^2}R,
 \end{aligned}$$

where the second inequality holds from Jensen's inequality, and the last inequality is due to Lemma A.3. This completes the proof. Compare to Ding et al. (2024a, Proposition 3.2).  $\square$

**Theorem 5.4.** Let Assumption 1 be fulfilled. For every  $t \in (0, 1)$ , it holds

$$\|\nabla u(t, x_t)\|_{\text{op}} \leq G, \quad x_t \in \mathbb{R}^d,$$

where  $G$  is a constant only depending on  $\sigma$  and  $R$ .

*Proof.* According to (3.3) and Lemmas A.1 and A.3, we have

$$\begin{aligned}
 \nabla u(t, x_t) &= -\frac{1}{1-t}\mathbf{I}_d + \frac{1}{1-t}\nabla\mathbb{E}[X_1|X_t = x_t] \\
 &= -\frac{1}{1-t}\mathbf{I}_d + \frac{1}{1-t}\frac{t}{(1-t)^2}\text{Cov}(X_1|X_t = x_t) \\
 &= -\frac{1}{1-t}\mathbf{I}_d + \frac{1}{1-t}\frac{t}{(1-t)^2}\frac{\sigma_t^4}{\sigma^4}\text{Cov}(Y_t^{x_t}) + \frac{1}{1-t}\frac{t}{(1-t)^2}\sigma_t^2\mathbf{I}_d \\
 &= \frac{\sigma^2t^2 - (1-t)}{\sigma^2t + (1-t)^2}\mathbf{I}_d + \frac{(1-t)t}{(\sigma^2t^2 + (1-t)^2)^2}\text{Cov}(Y_t^{x_t}).
 \end{aligned}$$

Then using triangular inequality yields

$$\begin{aligned}
 \|\nabla u(t, x_t)\|_{\text{op}} &\leq \frac{\sigma^2t^2 - (1-t)}{\sigma^2t + (1-t)^2} + \frac{(1-t)t}{(\sigma^2t^2 + (1-t)^2)^2}\|\text{Cov}(Y_t^{x_t})\|_{\text{op}} \\
 &\leq \frac{\sigma^2t^2 - (1-t)}{\sigma^2t + (1-t)^2} + \frac{(1-t)t}{(\sigma^2t^2 + (1-t)^2)^2}R,
 \end{aligned}$$

where the first inequality holds from the triangular inequality, and the last inequality is due to Lemma A.3. This completes the proof. See also Ding et al. (2024a, Proposition 3.5).  $\square$

**Proposition 6.2.** Suppose that  $\pi \in C^2(\mathbb{R}^d)$ . Assume further  $P(\theta) \succeq 0$  for each  $\theta \in \mathbb{R}^d$ . Then the invariant distribution of the preconditioned Langevin diffusion (6.2) is the same as that of the vanilla Langevin diffusion (6.1).

*Proof.* Let  $\pi_t$  be the density of the preconditioned Langevin diffusion  $\theta_t$  (6.2). The Fokker-Planck equation associated with SDE (6.2) is given as

$$\begin{aligned}\partial_t \pi_t(\theta) &= -\operatorname{div}((P(\theta)\nabla \log \pi(\theta) + \operatorname{div} P(\theta))\pi_t(\theta)) + \operatorname{div} \operatorname{div}(P(\theta)\pi_t(\theta)) \\ &= -\operatorname{div}(P(\theta)\nabla \log \pi(\theta)\pi_t(\theta)) + \operatorname{div}(P(\theta)\nabla \pi_t(\theta)) \\ &= \operatorname{div}\left(P(\theta)\left(\pi_t(\theta)\nabla \log \frac{\pi_t(\theta)}{\pi(\theta)}\right)\right).\end{aligned}$$

Since  $P(\theta) \succeq 0$  for each  $\theta \in \mathbb{R}^d$ , setting  $\partial_t \pi_t(\theta) = 0$  implies  $\pi_\infty = \pi$ . This completes the proof.  $\square$

## C Velocity Estimator for Time Close to One

In this section, we show how to avoid the factor  $\frac{1}{1-t}$  in the computation of the velocity field estimator  $\hat{u}$ . More specifically, we will see that

$$u(t, x_t) = \frac{1}{t}x_t + \frac{1-t}{t^2}\mathbb{E}_{X_1 \sim p_{X_1|X_t=x_t}} [\nabla \log p_{X_1}(X_1)].$$

To this end, consider, slightly more general than in (3.1), the probability path defined by the stochastic interpolant

$$X_t = \alpha_t X_0 + \beta_t X_1.$$

The vector field  $u(t, x_t)$  generating the marginal probability path is given by the conditional expectation of the velocity

$$u(t, x_t) = \mathbb{E}[\dot{X}_t \mid X_t = x_t],$$

and computing the time derivative of the interpolant yields

$$\dot{X}_t = \dot{\alpha}_t X_0 + \dot{\beta}_t X_1.$$

To evaluate the expectation conditioned on  $X_t = x_t$ , we eliminate the dependence on  $X_0$  by using the relation  $X_0 = (x_t - \beta_t X_1)/\alpha_t$  which results in

$$\dot{X}_t = \dot{\alpha}_t \left( \frac{x_t - \beta_t X_1}{\alpha_t} \right) + \dot{\beta}_t X_1 = \frac{\dot{\alpha}_t}{\alpha_t} x_t + \left( \dot{\beta}_t - \frac{\dot{\alpha}_t \beta_t}{\alpha_t} \right) X_1.$$

Taking the conditional expectation with respect to  $X_t = x_t$  gives the well known formula

$$(C.1) \quad u(t, x_t) = \frac{\dot{\alpha}_t}{\alpha_t} x_t + \left( \dot{\beta}_t - \frac{\dot{\alpha}_t \beta_t}{\alpha_t} \right) \mathbb{E}[X_1 \mid X_t = x_t].$$

This formulation is numerically unstable at  $t = 1$ , since usually  $\alpha_t \rightarrow 0$  as  $t \rightarrow 1$ . In the following, we will reformulate the expression of  $u$  such that we can get rid of  $\alpha_t$  as denominator.

To evaluate  $\mathbb{E}[X_1 \mid X_t = x_t]$ , we express the expectation as an integral over the posterior density using the target score, similarly to (Akhound-Sadegh et al., 2024, Equation 9). Using Bayes' theorem, the posterior density  $p_{X_1|X_t=x_t}$  is given by

$$p_{X_1|X_t=x_t}(x_1) = \frac{p_{X_t|X_1=x_1}(x_t)p_{X_1}(x_1)}{p_{X_t}(x_t)} = \frac{1}{p_{X_t}(x_t)} \gamma_{\alpha_t^2}(x_t - \beta_t x_1) p_{X_1}(x_1).$$

Let  $G(x_1, x_t) := \gamma_{\alpha_t^2}(x_t - \beta_t x_1)$ . Then the gradient reads as

$$\nabla_{x_1} G = G \cdot \left( -\frac{1}{2\alpha_t^2} \right) \nabla_{x_1} \|x_t - \beta_t x_1\|^2 = G \cdot \frac{\beta_t}{\alpha_t^2} (x_t - \beta_t x_1).$$

Rearranging gives the identity  $(x_t - \beta_t x_1)G = \frac{\alpha_t^2}{\beta_t} \nabla_{x_1} G$ . Now we can compute the conditional expectation by integrating against the posterior density, namely

$$\begin{aligned} \mathbb{E}[x_t - \beta_t X_1 \mid X_t = x_t] &= \int (x_t - \beta_t x_1) p_{X_1 \mid X_t = x_t}(x_1) \, dx_1 \\ &= \frac{1}{p_{X_t}(x_t)} \int (x_t - \beta_t x_1) G(x_1, x_t) p_{X_1}(x_1) \, dx_1 \\ &= \frac{1}{p_{X_t}(x_t)} \frac{\alpha_t^2}{\beta_t} \int (\nabla_{x_1} G) p_{X_1}(x_1) \, dx_1. \end{aligned}$$

Applying integration by parts (assuming vanishing boundary terms) yields

$$\begin{aligned} \frac{\alpha_t^2}{\beta_t p_{X_t}(x_t)} \int (\nabla_{x_1} G) p_{X_1} \, dx_1 &= -\frac{\alpha_t^2}{\beta_t p_{X_t}(x_t)} \int G(\nabla_{x_1} p_{X_1}) \, dx_1 \\ &= -\frac{\alpha_t^2}{\beta_t} \int \frac{G p_{X_1}}{p_{X_t}(x_t)} \nabla \log p_{X_1} \, dx_1 \\ &= -\frac{\alpha_t^2}{\beta_t} \int p_{X_1 \mid X_t = x_t}(x_1) \nabla \log p_{X_1}(x_1) \, dx_1 \\ &= -\frac{\alpha_t^2}{\beta_t} \mathbb{E}[\nabla \log p_{X_1}(X_1) \mid X_t = x_t], \end{aligned}$$

and consequently

$$x_t - \beta_t \mathbb{E}[X_1 \mid X_t = x_t] = -\frac{\alpha_t^2}{\beta_t} \mathbb{E}[\nabla \log p_{X_1}(X_1) \mid X_t = x_t].$$

Finally, solving for  $\mathbb{E}[X_1 \mid X_t = x_t]$ , we get

$$\mathbb{E}[X_1 \mid X_t = x_t] = \frac{1}{\beta_t} x_t + \frac{\alpha_t^2}{\beta_t^2} \mathbb{E}[\nabla \log p_{X_1}(X_1) \mid X_t = x_t].$$

Substituting the expression for  $\mathbb{E}[X_1 \mid X_t = x_t]$  into (C.1) we obtain for the *Linear term* ( $x_t$ ):

$$C_x = \frac{\dot{\alpha}_t}{\alpha_t} + \left( \dot{\beta}_t - \frac{\dot{\alpha}_t \beta_t}{\alpha_t} \right) \frac{1}{\beta_t} = \frac{\dot{\alpha}_t}{\alpha_t} + \frac{\dot{\beta}_t}{\beta_t} - \frac{\dot{\alpha}_t}{\alpha_t} = \frac{\dot{\beta}_t}{\beta_t},$$

*Score term* ( $S$ ):

$$C_S = \left( \frac{\alpha_t \dot{\beta}_t - \dot{\alpha}_t \beta_t}{\alpha_t} \right) \frac{\alpha_t^2}{\beta_t^2} = \frac{\alpha_t(\alpha_t \dot{\beta}_t - \dot{\alpha}_t \beta_t)}{\beta_t^2}.$$

**Final Result.** Putting everything together we obtain

$$u(t, x_t) = \frac{\dot{\beta}_t}{\beta_t} x_t + \frac{\alpha_t(\alpha_t \dot{\beta}_t - \dot{\alpha}_t \beta_t)}{\beta_t^2} \mathbb{E}_{X_1 \sim p_{X_1 \mid X_t = x_t}} [\nabla \log p_{X_1}(X_1)].$$

In particular, for the time schedule  $\alpha_t = 1 - t$  and  $\beta_t = t$ , we get

$$u(t, x_t) = \frac{1}{t} x_t + \frac{1-t}{t^2} \mathbb{E}_{X_1 \sim p_{X_1 \mid X_t = x_t}} [\nabla \log p_{X_1}(X_1)].$$

## D Preconditioning

Algorithms 4 and 5 present the preconditioned counterparts of Algorithms 1 and 2, respectively. They detail the procedures for velocity estimation and initialization using preconditioned Langevin algorithms, which are discrete-time approximations of the preconditioned Langevin diffusion (6.2).

---

**Algorithm 4:** Monte Carlo-based velocity estimation with preconditioning

---

**Input:** The location of interest  $x_t$ , the target score  $\nabla \log p_{X_1}$ , the step size  $\eta$ , the number of steps  $K$ , the smoothing constant  $\alpha$ , and the tolerance  $\epsilon$  for numerical stability.

**Output:** A Monte Carlo-based estimation  $\hat{u}(t, x_t)$ .

```

1 Initialize particles:  $\bar{Z}_0^1, \dots, \bar{Z}_0^n$ .
2 Initialize the variance  $v_0^i \leftarrow 0$  for  $1 \leq i \leq n$ .
3 for  $k \in \{0, \dots, K-1\}$  do
4   # Calculate denoising score
5    $s_{k+1}^i \leftarrow -\frac{t^2}{(1-t)^2} \bar{Z}_{k\eta}^i + \frac{t}{(1-t)^2} x_t + \nabla \log p_{X_1}(\bar{Z}_{k\eta}^i)$  for  $1 \leq i \leq n$ .
6   # Preconditioned Langevin update
7    $v_{k+1}^i \leftarrow \alpha v_k^i + (1-\alpha)s_{k+1}^i \odot s_{k+1}^i$  for  $1 \leq i \leq n$ .            $\triangleright$  Moving average
8    $P_{k+1}^i \leftarrow \text{diag}(1/(\sqrt{v_{k+1}^i} + \epsilon))$  for  $1 \leq i \leq n$ .            $\triangleright$  Preconditioner
9    $\bar{Z}_{(k+1)\eta}^i \sim \mathcal{N}(\bar{Z}_{k\eta}^i + \eta P_{k+1}^i s_{k+1}^i, 2\eta P_{k+1}^i)$  for  $1 \leq i \leq n$ .            $\triangleright$  Langevin update
10 end
11 # Monte Carlo estimation
12  $\hat{u}(t, x_t) \leftarrow -\frac{1}{1-t} x_t + \frac{1}{1-t} \frac{1}{n} \sum_{i=1}^n \bar{Z}_{K\eta}^i$ .
13 return  $\hat{u}(t, x_t)$ 

```

---

## E Experimental Details and Additional Experimental Results

### E.1 Experimental details.

**Hyper-parameters of SSI.** The hyper-parameters of SSI are summarized in Table 2. The two-dimensional target distributions `rings`, `MoG7x7`, and `MoG40` are studied in Section 7.1, the eight-dimensional distribution `ManyWell` is investigated in Section 7.2, while `Bayesian` represents Bayesian inference in Section 7.3.

For the hyper-parameters of probability flow ODE (PF ODE), consistent with Algorithm 3,  $T_0$  and  $T_{\text{end}}$  denote the initialization and early-stopping times, respectively, while  $M$  represents the number of discretization steps in (5.5). Regarding the PF ODE initialization in Algorithm 2,  $\tau$  and  $L$  correspond to the step size and number of steps of the Langevin Monte Carlo in (5.3). Similarly, for score estimation,  $\eta$  and  $K$  denote the step size and number of steps of the Langevin Monte Carlo in (4.2). Furthermore, to reduce the computational cost, we execute Langevin Monte Carlo chains in parallel and utilize samples obtained after convergence. Consequently,  $n$  denotes the total number of Monte Carlo particles in velocity estimation as (4.7), calculated as the product of the number of chains and the sampling steps retained after the warm up period in each chain.

**Hyper-parameters of baselines.** We compared our method against ULA, MALA, pULA, and HMC in Sections 7.1 and 7.2.

We report the step size  $\eta$ , and the number of steps  $N$  for each method in Table 3. In

**Algorithm 5:** Initialization of probability flow ODE with preconditioning

---

**Input:** The step size  $\tau$ , the number of steps  $L$ , the smoothing constant  $\alpha$ , and the tolerance  $\epsilon$  for numerical stability.

**Output:** Particle  $\hat{U}_{L\tau}$  approximately following  $p_{X_{T_0}}$ .

```

1 Initialize particle:  $\hat{U}_0$ .
2 Initialize the variance  $v_0 \leftarrow 0$ .
3 for  $\ell \in \{0, \dots, L-1\}$  do
4   # Score estimation
5   Calculate the velocity estimator  $\hat{u}(T_0, \hat{U}_{\ell\tau})$  using Algorithm 1.
6   Calculate the score estimator  $\hat{s}_{\ell+1} := \hat{s}(T_0, \hat{U}_{\ell\tau})$  using (5.2).
7   # Preconditioned Langevin update
8    $v_{\ell+1} \leftarrow \alpha v_\ell + (1 - \alpha) \hat{s}_{\ell+1} \odot \hat{s}_{\ell+1}$ . ▷ Moving average
9    $P_{\ell+1} \leftarrow \text{diag}(1/(\sqrt{v_{\ell+1}} + \epsilon))$ . ▷ Preconditioner
10   $\hat{U}_{(\ell+1)\tau} \sim \mathcal{N}(\hat{U}_{\ell\tau} + \tau P_{\ell+1} \hat{s}_{\ell+1}, 2\tau P_{\ell+1})$ . ▷ Langevin update
11 end
12 return  $\hat{U}_{L\tau}$ 

```

---

Table 2: Hyper-parameters of SSI.

dim.	PF ODE			Initialization			Score estimation				
	$T_0$	$T_{\text{end}}$	$M$	$\tau$	$L$	precond.	$\eta$	$K$	$n$	precond.	
rings	2	0.2	0.99	100	0.1	100	✗	0.01	100	800	✗
MoG7x7	2	0.2	0.99	100	0.1	100	✓	0.01	100	800	✓
MoG40	2	0.2	0.99	100	0.1	100	✓	0.01	100	800	✓
ManyWell	8	0.6	0.99	100	0.1	100	✓	0.01	100	800	✓
Bayesian	4	0.8	0.99	20	0.01	50	✗	0.01	20	80	✗

Table 3: Hyper-parameters of baselines.

dim.	ULA		MALA		pULA		HMC		
	$\eta$	$N$	$\eta$	$N$	$\eta$	$N$	$\eta$	$N$	
Rings	2	0.05	10,000	0.1	10,000	0.5	10,000	0.05	100×100
MoG7x7	2	0.1	10,000	0.1	10,000	0.1	10,000	1.0	100×100
MoG40	2	0.5	50,000	0.5	50,000	0.5	50,000	1.0	100×100

particular, for HMC, we consistently used a trajectory of 100 transitions with 100 leapfrog steps per transition across all tasks, which means  $N = 100 \times 100$  of steps in total.

**Ablation Studies.** We performed ablation studies on the MoG7x7 task ( $d = 2$ ) to analyze the impact of the initialization time  $T_0$  and the benefits of preconditioning. The initialization time was varied across the set  $T_0 \in \{0.01, 0.1, 0.2, 0.3, 0.4, 0.5, 0.6, 0.7, 0.8, 0.9\}$ . Consistent with our implementation, for  $T_0 < 0.05$  (i.e.,  $T_0 = 0.01$ ), the number of outer Langevin steps was set to  $L = 0$ , effectively reducing the initialization to a standard Gaussian sample. For  $T_0 \geq 0.05$ , we employed the hyper-parameters listed for MoG7x7 in Table 2, while specifically comparing the standard preconditioned setting against a non-preconditioned baseline.

**E.2 Additional experimental results.** In this subsection, we compare our method with a neural sampler [Máté and Fleuret \(2023\)](#). Specifically, the method leverages the continuity equation:

$$\partial_t f_t - \underbrace{\mathbb{E}_{p_{X_t}}[\partial_t f_t]}_{A_t} = -\langle \nabla f_t, u(t, x) \rangle + \nabla \cdot u(t, x),$$

where the density is defined as  $p_{X_t}(x) = e^{-f_t(x)}/Z_t$  for  $Z_t := \int e^{-f_t(x)} dx$ . To solve this, the potential  $f_t$  is parameterized as an interpolation  $f_t = t f_1 + (1-t) f_0 + t(1-t) \phi_t$ , where  $\phi_t$  is approximated by a neural network  $\phi_t^\theta$ . The optimization objective is formulated as:

$$\mathcal{L}(\theta) = \mathbb{E}_{t \sim \mathcal{U}[0,1], z \sim p_0} \left[ \left| \partial_t f_t^{\theta_1} - A_t^{\theta_2} + \langle \nabla f_t^{\theta_1}, u^{\theta_3}(t, x) \rangle - \nabla \cdot u^{\theta_3}(t, x) \right| \right],$$

where  $\theta = (\theta_1, \theta_2, \theta_3)$  represents the trainable parameters. Since the approximation of high-dimensional integrals over the intermediate density  $p_{X_t}$  is computationally intractable, [Máté and Fleuret \(2023\)](#) proposed an iterative optimization strategy. Let  $\theta'$  denote the parameters obtained from the previous minimization step. We solve the flow ODE  $\partial_t \psi_t^{\theta'} = u^{\theta'}(t, \psi_t^{\theta'})$  with the initial condition  $\psi_0^{\theta'} = \text{Id}$  using these fixed parameters  $\theta'$ . The loss is then evaluated on points generated by sampling  $z \sim p_0$  and then applying  $\psi_t^{\theta'}$ . Figure 8 illustrates the experimental results on the `rings`, MoG7x7, and MoG40 datasets.

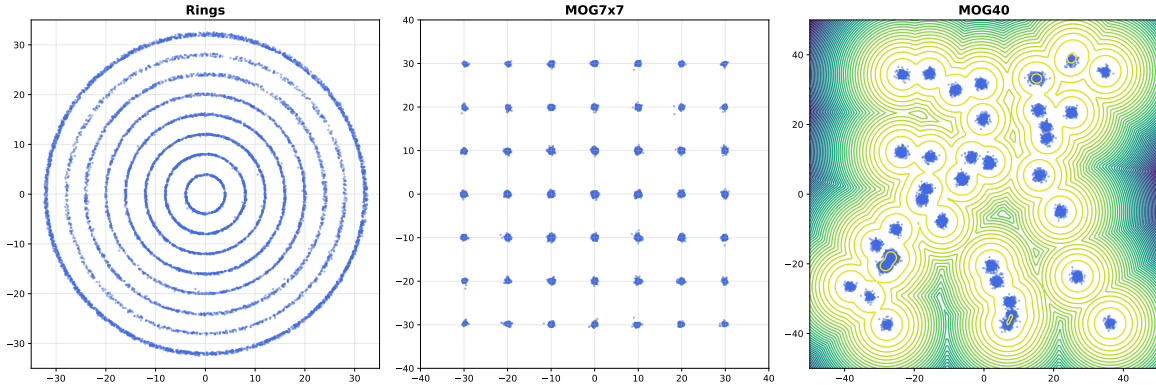


Figure 8: Results for the neural sampling.

For these experiments, we utilized the training configuration with consistent hyper-parameters across all three datasets. The training process used a batch size of 4096, a learning rate of  $1.0 \times 10^{-3}$ , and a decay rate of 0.98. The total training duration was set to  $N_{\text{train}} = 30,000$  steps, utilizing 51 inner steps for the flow integration. We initialized the noise level at  $\sigma = 20.0$  and set the generalized Gaussian exponent to  $p = 2.0$  (corresponding to a standard Gaussian).